University of Leoben

Dissertation

Damage tolerance and strength increase of drivetrain components

Dipl.-Ing. Jürgen Maierhofer

Materials Center Leoben Forschung GmbH

Erich Schmid Institute of Materials Science
Austrian Academy of Science

Leoben, May 2014

Financial support by the Austrian Federal Government (in particular from the Bundesministerium für Verkehr, Innovation und Technologie and the Bundesministerium für Wirtschaft, Familie und Jugend) and the Styrian Provincial Government, represented by Österreichische Forschungsförderungsgesellschaft mbH and by Steirische Wirtschaftsförderungsgesellschaft mbH, within the research activities of the K2 Competence Centre on "Integrated Research in Materials, Processing and Product Engineering", operated by the Materials Center Leoben Forschung GmbH in the framework of the Austrian COMET Competence Centre Programme, is gratefully acknowledged.

Materials Center Leoben Forschung GmbH
Roseggerstraße 12
8700 Leoben
Austria

Affidavit

I declare in lieu of oath,
that I wrote this thesis
and performed the associated research myself,
using only literature cited in this volume.

_____

Jürgen Maierhofer

Leoben, May 2014

Ausdauer wird früher oder später belohnt –
meistens aber später

Wilhelm Busch

Acknowledgements

Ich möchte mich bei allen Personen, die mir in den letzten drei Jahren mit Rat und Tat zur Seite gestanden sind und die somit zum Gelingen dieser Dissertation beigetragen haben, bedanken.

Mein großer Dank gilt meinem Betreuer Prof. Reinhard Pippan, der mir bei sämtlichen Fragestellungen mit seinem umfangreichen Wissen immer wieder weiterhelfen konnte, und dessen Büro ich immer wieder mit einem neuem Motivationsschub verließ.
Besonderen Dank möchte ich auch Hans-Peter Gänser aussprechen, der mir in kollegialer Art und Weise die schadenstolerante Auslegung von Bauteilen näherbrachte und mir beim Leiten des Projektes immer wieder unter die Arme gegriffen hat.
Ich werde die vielen gemeinsamen Treffen mit Reinhard und Hans-Peter, welche an Hand zahlreicher interessanter Diskussionen wesentlichen Anteil am Erfolg dieser Dissertation hatten, immer in guter Erinnerung behalten.

Die vorliegende Dissertation wurde im Rahmen des COMET K2 Projektes A4.13 Schadenstoleranz und Festigkeitssteigerung von Radsatzwellen am Materials Center Leoben Forschung GmbH sowie am Erich Schmid Institut für Materialwissenschaften der österreichischen Akademie der Wissenschaften durchgeführt. Für die Möglichkeit zur Durchführung dieser Dissertation möchte ich mich bei Prof. Reinhold Ebner und Werner Ecker bedanken.

Stellvertretend für sämtliche Firmen und Institute die im Rahmen dieses Projektes Produkte, Dienstleistungen oder Informationen zum Gelingen des Projektes beigetragen haben möchte ich mich bei Guntram Rüf (Fa. Siemens), Helmut Hochbein (Fa. Hegenscheidt), Thomas Christiner (Lehrstuhl für Allgemeinen Maschinenbau), Thomas Antretter (Institut für Mechanik), Herrn Fimbinger (Fa. Fimbinger) und Herrn Dornhofer (Fa. Petschenig) für die gute Zusammenarbeit bedanken.

Ich danke dem Verantwortlichen für die Werkstatt des Erich Schmid Instituts Franz Hubner für das Fertigen sämtlicher Versuchsproben und Einspannvorrichtungen, sowie dem Verantwortlichen für die Prüfhalle Peter Kutlesa für die reibungslose Zusammenarbeit.

Zusätzlich möchte ich mich bei Beiden für die aufheiternden Gespräche und Diskussionen bedanken, sie machten die Zeit in der Prüfhalle bzw. in der Werkstatt zu einer angenehmen Abwechslung.

Des Weiteren möchte ich mich bei meinen Bürokollegen Martin Smolka, Alexander Wimmer, Mario Stefenelli, Peter Gruber, Robert Peissl, Ronald Schöngrundner, Walter Ochensberger, Masoud Sistaninia, Xiang Zhou, Darjan Kozic, Stefan Kolitsch, Ivan Zivkovic, Lisa Schnur und Thomas Kaltenbrunner für das angenehme Arbeitsklima bedanken.

Letztendlich möchte ich mich bei sämtlichen nicht namentlich erwähnten Mitarbeitern am MCL sowie am Erich Schmid Institut für die gute Zusammenarbeit bedanken.

Ganz besonderer Dank gilt natürlich auch meinen Eltern Margaretha und Otto Maierhofer, welche mir eine höhere Schulbildung überhaupt erst ermöglichten. Auch meinen Geschwistern Cornelia, Otto, Wolfgang, Markus, Martin, Oliver und Alex, sowie meinen Schwiegereltern, meinen Schwagern und Schwägerinnen, meinen Nichten und Neffen und meinen Freunden möchte ich für die moralische Unterstützung danken.

Der mit Sicherheit größte Dank gebührt allerdings meiner Frau Maria und meinen Kindern Gabriel und Lorena, ohne Euch wäre das nicht möglich gewesen, Ihr seid mein größter Rückhalt und mein wichtigster Antrieb.

Abstract

For the damage tolerant design of components, the external load and the component's geometry as well as residual stresses and defects such as cracks or non-metallic inclusions are of importance. The load carrying capacity is given for long-term fatigue endurance by the crack growth threshold, for finite lifetime by the fatigue crack growth rate; both depend on the load ratio, but also on the size of the defect.

In this work the fatigue crack growth behaviour of the quenched and tempered steel 25CrMo4 is investigated in detail by means of single edge notched bending (SENB) specimens at various load ratios. The influence of flaw size is studied by different notch depths. At the notch root, short fatigue cracks are introduced by cyclic compression. The growth behaviour of these cracks in the notch stress field is monitored in detail, whereby also information about the build-up of crack closure and the transition from short to long crack behaviour is gained. In order to investigate the influence of compressive residual stresses – as introduced by various mechanical surface treatment processes such as shot peening or deep rolling – straight beams with convex fillets are subjected to controlled flat rolling, thereby introducing residual stresses varying along the ligament of the specimen. In these specimens, again fatigue cracks are introduced and monitored, showing the combined influence of residual stresses and crack length on the fatigue crack growth behaviour. In all cases, special attention is paid to the evolution of the fatigue crack growth threshold as a function of crack length, stress ratio and residual stresses.

Based on the evolution of the fatigue crack growth threshold as a function of crack length (crack resistance curve), an analytical model for describing the fatigue crack growth rate, as well as an extended Kitagawa-Takahashi diagram are developed. The model is based on the NASGRO equation, which is modified to describe the build-up of crack closure with increasing crack length and thereby the short crack behaviour. With this extended NASGRO model it is possible, due to a combined view of load stresses and residual stresses, to describe the crack growth also in the presence of residual stresses.

In summary, the results of this work provide a more accurate way to estimate the lifetime or service intervals of cyclically loaded components in the presence of flaws and residual stress fields.

Kurzfassung

Für die schadenstolerante Auslegung von Bauteilen sind sowohl die äußere Last und die Bauteilgeometrie als auch äußere Defekte wie z.B. Risse, innere Defekte und Eigenspannungen von Bedeutung. Die lastabhängige Tragfähigkeit für einen dauerfest ausgelegten Bauteil ist durch den Schwellwert für Risswachstum, für Zeitfestigkeit durch die Rissfortschrittsrate, gegeben. Beide sind abhängig vom Lastverhältnis, aber auch von der Größe des Defektes.

In dieser Arbeit wird das Wachstumsverhalten von Ermüdungsrissen im Vergütungsstahl 25CrMo4 mittels Single Edge Notched Bending (SENB)-Proben für verschiedene Lastverhältnisse detailliert untersucht. Der Einfluss der Fehlergröße wird anhand unterschiedlich tief eingebrachter Kerben untersucht. Am Kerbgrund werden durch zyklisches Anschwingen unter Druck kurze Ermüdungsrisse initiiert. Das Risswachstumsverhalten im Spannungsfeld dieser Kerben wird genauestens untersucht, wobei man zusätzlich Informationen über das Aufbauen von Rissschließeffekten sowie über den Übergang von Kurz- zu Langrissverhalten erhält. Um den Einfluss von Druckeigenspannungen – welche durch diverse oberflächenverfestigende Verfahren wie Festwalzen oder Kugelstrahlen eingebracht werden können – auf das Risswachstumsverhalten zu untersuchen, wurde in Flachproben durch kontrolliertes Walzen ein Eigenspannungsfeld eingebracht. In diesen Flachproben wurden anschließend abermals Kerben eingebracht und Ermüdungsversuche durchgeführt, um den kombinierten Einfluss von Eigenspannungen und Risslänge auf das Verhalten von Ermüdungsrissen zu zeigen. In allen Fällen wurde der Entwicklung des Schwellwertes für Ermüdungsrisswachstum als einer Funktion von Risslänge, Lastverhältnis und Eigenspannungen besondere Beachtung geschenkt.

Basierend auf dem sich mit der Rissverlängerung aufbauenden Rissschließen (Risswiderstandskurve), wird ein analytisches Modell zum Beschreiben der Rissfortschrittsrate sowie ein erweitertes Kitagawa-Takahashi Diagramm entwickelt. Das Rissfortschrittsmodell basiert auf der NASGRO-Gleichung, welche um eine detaillierte Beschreibung des sich aufbauenden Rissschließens erweitert wird, um damit das Kurzrissverhalten zu berücksichtigen. Durch einen kombiniert betrachteten Einfluss von Last- und Eigenspannungen ist es mit diesem erweiterten NASGRO-Modell auch möglich, das Risswachstum in Eigenspannungsfeldern zu beschreiben.

Zusammenfassend ermöglichen die Ergebnisse dieser Arbeit eine genauere Abschätzung der Lebensdauer oder notwendiger Inspektionsintervalle zyklisch beanspruchter, fehler- und eigenspannungsbehafteter Bauteile.

Contents

1 Introduction

Surface treatment procedures such as deep rolling, shoot peening, laser shot peening etc. are one possibility to increase the lifetime of a cyclically loaded component. Such surface treatment procedures introduce high compressive residual stresses near the surface of the component and therefore increase the lifetime of this component especially in the presence of flaws, provided the flaw size is smaller than the influence of the introduced compressive residual stress field.

For damage tolerant fracture control concepts, especially for drivetrain components it is crucial to estimate the crack growth behaviour very accurately so that one can derive inspection intervals or estimate the criticality of an existing flaw also in the presence of residual stresses. State-of-the-art procedures for surface defects in drivetrain components are grinding out or re-working by turning within the framework of standard specifications. In the worst case the whole component must be taken out of operation.

If a crack grows from the root of a flaw, with increasing crack length the build-up of crack closure and therefore the resistance against crack propagation – the crack resistance curve – increases until, after a certain crack extension, the resistance against crack propagation remains constant. So even if there is no compressive residual stress field, it is possible that a crack after a certain crack extension is arrested and no further crack propagation occurs at an applied constant load. This effect is even more powerful in the presence of compressive residual stresses. So an accurate crack growth model, considering in detail the build-up of crack closure, in combination with a surface treated component can on one hand increase the safety of a component and on the other hand save enormous maintenance costs.

The goals of this thesis are

- to develop an empirical formula to estimate the depth of compressive residual stresses introduced by deep rolling, dependent on rolling force and geometry of the rolling tool,
- to determine a crack growth model which can predict the growth rate for cracks of arbitrary length in the presence of residual stresses and finally
- to estimate the endurance limit and/or the lifetime of a component containing flaws and residual stresses.

By achieving these goals it will therefore be possible, in the context of damage tolerant design, to predict fatigue lifetime or necessary inspection intervals more accurately even for small flaws in the presence of residual stresses.

The thesis starts with a short background overview on the mechanical behaviour of fatigue cracks. The somewhat strange behaviour of short cracks and it's physical explanation is elucidated in detail. Afterwards an introduction to deep rolling, a very effective mechanical surface treatment process, for introducing compressive residual stresses in a component is given; in this context, also a simple model to predict the stability of such residual stresses during operation is proposed. Subsequently, the methods used in this thesis for measuring residual stress fields (X-ray diffraction, Cut-Compliance method) are explained in detail. An introduction to the three major fracture control concepts complements the background overview. Section 3 presents a short summary of the main results of the thesis, followed by a detailed account in the form of published scientific articles.

2 Background

2.1 Crack growth behaviour under cyclic loading

2.1.1 Griffith energy concept

The energy concept according to Griffith [Gri20] is based on the first law of thermodynamics, which states that the total energy of an isolated system is constant. That implies that energy cannot be destroyed or created, the energy can only be transformed from one type to another. Griffith applied this idea to the formation of a crack. He supposed that the total potential energy U of a body must decrease at instable crack extension:

$$\frac{dU}{da} = \frac{d\left(U_{el} - U_w + U_O\right)}{da} \leq 0 \tag{1}$$

The contributions to the total potential energy U are the elastic energy U_{el}, the work done by the external forces U_w and the work required to create new surfaces U_O. A restated formulation of the Griffith idea is that energy provided from the elastic stress field and the work of the external forces must be greater or equal than the energy for creating a fracture surface. This provided energy is also called energy release rate G, the energy for creating a fracture surface is called crack resistance R.

$$G = -\frac{d\left(U_{el} - U_w\right)}{da} \geq \frac{dU_O}{da} = R \tag{2}$$

That implies that the criterion for instable crack growth can now be formulated as $G \geq R$. The energy release rate G depends only on the component geometry, the crack length and the applied load. G is apart from the young's modulus E material-independent, whereas the crack resistance R depends only on the material and optionally on the environment [Pip11].

In an ideally brittle solid, as supposed in Griffith's energy concept, a crack can be formed by breaking atomic bonds. However, when a crack propagates through a metal, also plastic deformation in the vicinity of the crack tip occurs. If this plastic deformation zone around the crack tip is small in comparison to the component size and to the crack length, we are talking about small scale yielding.

If the conditions for small scale yielding are fulfilled, then the conversion of elastic energy due to crack propagation is approximately the same as the conversion of elastic energy for ideally brittle fracture. Therefore, the energy release rate for small scale yielding conditions is

similar to the energy release rate for ideally brittle fracture. However, the crack resistance for these situations is different. In the ideally brittle case only the fracture surface energy has to be expended, whereas in the case of small scale yielding the plastic deformation energy must be expended in addition.

Because the relations for the energy release rate and also the conditions for fracture are the same (only the resistance against crack propagation differs) as in the ideally brittle case, this is referred as linear elastic fracture mechanics (LEFM).

2.1.2 Linear elastic fracture mechanics

In fracture mechanics one distinguishes between three different modes of loading (Fig. 2.1):

Mode I (opening): Load is applied normal to the plane of the crack.

Mode II (in-plane shear): Crack faces are sheared in a direction normal to the crack front.

Mode III (out-of-plane shear): Crack faces are sheared parallel to the crack front.

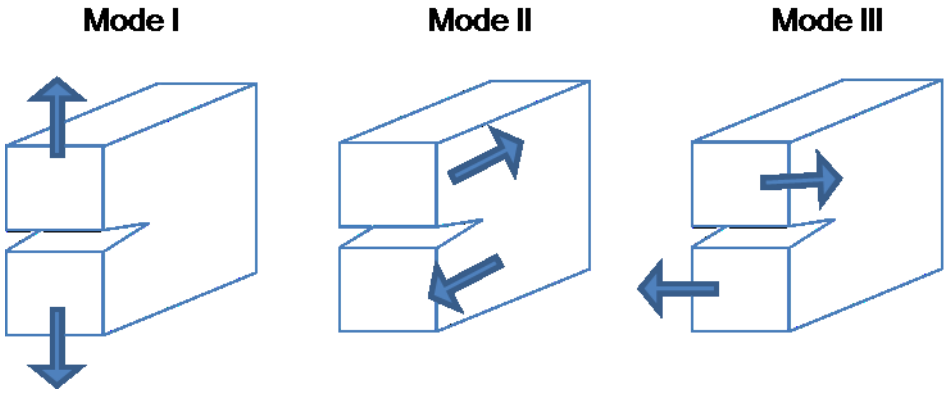

Fig. 2.1 Three basic modes of loading that can be applied to a crack.

In contrast to Griffith's energy concept, Irwin [Irw57] quantified the near-tip field for the linear elastic crack in terms of the stress intensity factor K. So it was possible to formulate the critical conditions for crack propagation in more precise terms by means of linear elastic stress analyses [Sur98].

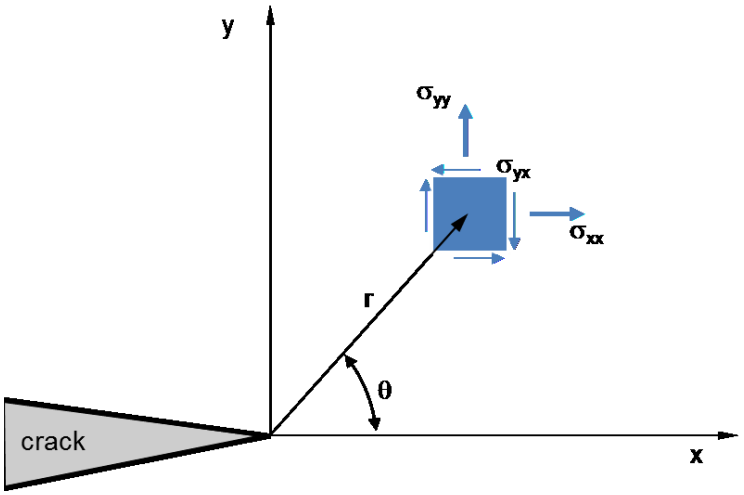

Fig. 2.2 Coordinate system and stresses at the crack front.

The different components of the stress tensor σ_{ij} can be calculated as a function of the distance r (see Fig. 2.2) from the notch tip by

$$\sigma_{ij} = \left(\frac{k}{\sqrt{r}}\right) \cdot f_{ij}(\theta) + \sum_{m=0}^{\infty} A_m r^{\frac{m}{2}} g_{ij}^{(m)}(\theta), \tag{3}$$

where k is a constant and f_{ij} is a dimensionless function of θ in the leading term. For the higher-order terms, A_m is the amplitude and $g_{ij}^{(m)}$ is a dimensionless function of θ for the m^{th} term [And05]. In the vicinity of the crack tip, the second term in equation (3) can be neglected. However, this term is very important for deciding the crack path through a component. The leading term in equation (3) describes for each mode of loading a stress singularity with $1/\sqrt{r}$ at the crack tip, only the constants k and f_{ij} depend on the loading mode. It is convenient at this point to replace k by the stress intensity factor K, where $K = k \cdot \sqrt{2 \cdot \pi}$. Thus, the stress field ahead of a crack tip in an isotropic linear elastic material, for Mode I loading, can be written as [And05]:

$$\lim_{r \to 0} \sigma_{ij}^{(\mathrm{I})} = \frac{K_{\mathrm{I}}}{\sqrt{2\pi r}} \cdot f_{ij}^{(\mathrm{I})}(\theta). \tag{4}$$

In most cases the stress intensity factor K can be written as

$$K = \sigma \cdot \sqrt{\pi \cdot a} \cdot Y\left(\frac{a}{w}\right), \tag{5}$$

where σ is the nominal stress, a is the crack length and $Y(\frac{a}{w})$ is a geometric factor depending on the crack length and the component size. The solution for the geometric factor of various

geometries can be found in several books [Mur87, Wu91, Tad00, Fet08].
For practical applications the stress intensity factor concept is more often used than the energy concept. One essential reason for this is that for various geometries and load conditions the *K*-concept is easier to handle. Another reason is that the basic idea of a singularity at the crack tip is transferrable to non-linear material behaviour [Gro07].

2.1.3 Fatigue crack growth

Schijve [Sch09] divides the fatigue life of a component until failure into two periods: the crack initiation period and the crack growth period. The initiation period is supposed to be completed when microcrack growth depends no longer on the material surface conditions, or when crack growth resistance of the material is controlling the crack growth rate, respectively. The crack growth rate in a cyclically constant loaded component is expressed in terms of crack length increase per cycle, da/dN. Usually, the crack growth rate da/dN increases with increasing number of cycles, with some exceptions for short cracks as will be discussed later. For a constant cyclic load, the stress range $\Delta\sigma$ as well as the stress ratio R can be calculated using the minimum $\sigma_{\min}$ and maximum $\sigma_{\max}$ loads during one cycle:

$$\Delta\sigma = \sigma_{\max} - \sigma_{\min}, \qquad R = \frac{\sigma_{\min}}{\sigma_{\max}}. \tag{6}$$

In analogy to equation (6) the stress intensity factor range can be defined as

$$\Delta K = K_{\max} - K_{\min}. \tag{7}$$

$K_{\max}$ and $K_{\min}$ are the maximum and minimum stress intensity factors during one load cycle. Experimentally determined crack growth curves, plotted in a doubly logarithmic diagram, show a characteristic shape with three different regions (see Fig. 2.3). Region I is called the threshold region, region II is the Parisregion and region III is the transition region from stable to unstable crack growth.

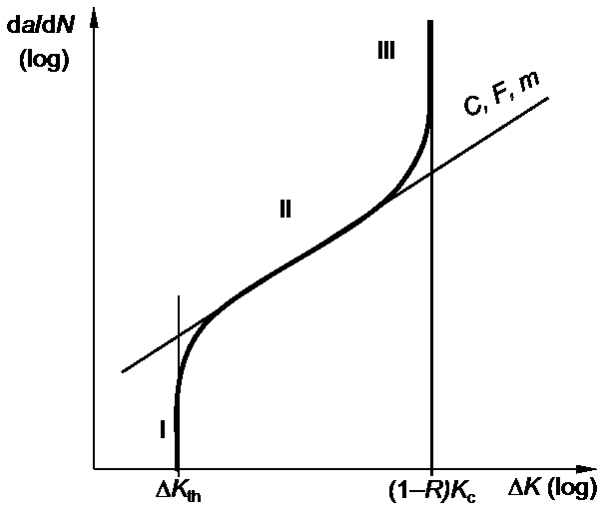

Fig. 2.3 Crack growth curve (long crack behaviour).

The relation of the crack growth rate d*a*/d*N* and the stress intensity factor range in the Parisregion can be described by the Parislaw [Par61, Par63]

$$\frac{da}{dN} = C \cdot (\Delta K)^m , \tag{8}$$

where C and m are material dependent constants. Many researchers have developed equations that model the whole crack growth curve (d*a*/d*N*-curve) or at least parts of it [For67, Kles72, McE88]. The most common expression is the so-called NASGRO equation published by Forman and Mettu [For92]:

$$\frac{\mathrm{d}a}{\mathrm{d}N} = C \cdot F \cdot \Delta K^m \cdot \frac{\left(1 - \frac{\Delta K_{\mathrm{th}}}{\Delta K}\right)^p}{\left(1 - \frac{K_{\max}}{K_{\mathrm{c}}}\right)^q}. \tag{9}$$

In comparison with equation (8) four additional material constants p, q, ΔK_{th} and K_{C} were added, whereby ΔK_{th} and K_{C} describe the location of branches I and III of the crack growth curve and p and q are a measure for the transition between the different branches. The multiplying factor F [For92, New84] considers the phenomenon of crack closure and therefore the stress ratio dependent crack growth rate in the Parisregion. Elber [Elb70] showed that for cyclic tension loading the fatigue crack is already closed before the minimum load is reached. Also with increasing load a fatigue crack stays closed until a certain load is reached.

This implies that not the whole stress intensity factor range, but only the effective stress intensity range

$$\Delta K_{\text{eff}} = K_{\text{max}} - K_{\text{op}}, \tag{10}$$

is responsible for crack propagation. The crack opening stress intensity factor K_{op} corresponds to the load where the crack starts to open. For high load ratios R the crack opening stress intensity factor K_{op} approaches the minimum stress intensity factor K_{min}. As a rule of thumb in particular, for load ratios $R > 0.7$ K_{op} is equal to K_{min} and ΔK_{eff} equals ΔK, i.e., no crack closure effects are present even for long cracks.

2.1.4 Short crack behaviour

Using Eq. (9) it is possible to fit the whole da/dN curve in dependence of the load ratio R. However, several works showed the somewhat strange behaviour of short cracks, which are able to propagate below the threshold for crack growth ΔK_{th}, and which are able to grow significantly faster than long cracks [Fro56, Pea75, Lan82, Tan83, Mil86, Now86, Rit86, Pip87a, Kit90, New99, Rad07].

Suresh and Ritchie [Sur84a] broadly classified the different kinds of short cracks into microstructurally short cracks, mechanically short cracks, physically short cracks and chemically short cracks. Microstructurally short cracks are comparable in size to the scale of the characteristic microstructural dimension. Mechanically short cracks are comparable to the near-tip plastic zone, or are engulfed by the plastic strain field of a notch. Physically short cracks are significantly larger than the characteristic microstructural dimension and the scale of local plasticity, and typically have lengths smaller than a millimetre or two in metals. Finally, chemically short cracks exhibit apparent anomalies in their propagation rate due to environmental corrosion effects.

For long crack behaviour there exists an unambiguous relation between the stress intensity factor range ΔK and the crack growth rate da/dN (see Fig. 2.3). Every deviation from this long crack behaviour may be summarized in terms of short crack behaviour, or in other words, for short cracks there exists no unique connection between ΔK and da/dN anymore (see Fig. 2.4).

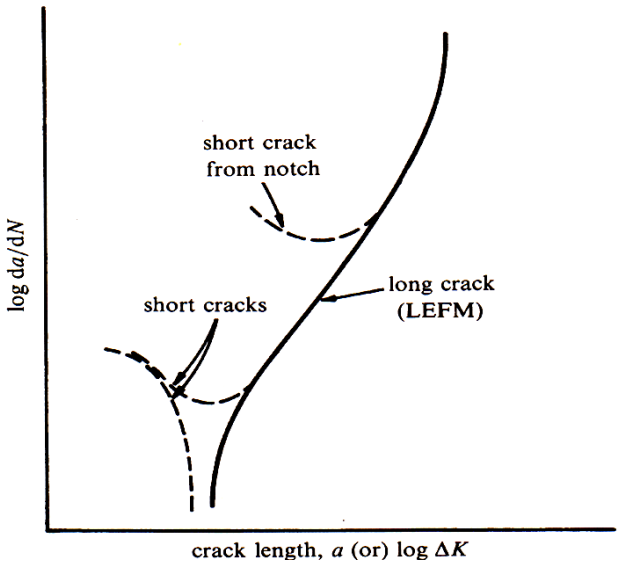

Fig. 2.4 Short crack behaviour [Sur98].

The reason for this different crack growth behaviour of short cracks is crack closure. There exist various different crack closure mechanisms (Fig. 2.5) categorized in the works by Suresh and Ritchie [Rit80, Sur81, Sur82a, Sur84b].

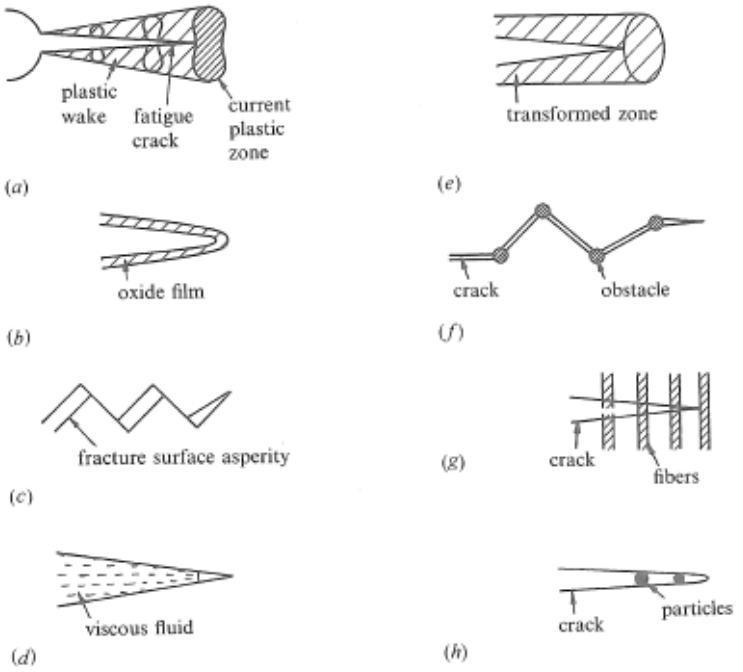

Fig. 2.5 Fatigue crack closure mechanisms [Sur98]. **a** plasticity-induced crack closure; **b** oxide-induced crack closure; **c** roughness-induced crack closure; **d** fluid-induced crack closure; **e** transformation-induced crack closure; **f** crack deflection; **g** crack-bridging by fibers; **h** crack-bridging (trapping) by particles.

These crack closure mechanisms are responsible for the build-up of crack resistance during crack propagation. The extent of the resistance against crack propagation depends on the crack extension length – the length where the crack surfaces can be in contact. For long cracks the crack closure mechanisms are built-up completely and the resistance against crack propagation reaches an upper limit, the long crack threshold $\Delta K_{th,lc}$. In contrast, for short cracks the crack closure mechanisms are not built-up completely and so also the resistance against crack propagation is smaller. This implies that short cracks are able to propagate below the threshold of long cracks and that they can grow significantly faster than long cracks at the same stress intensity factor range.

In this work only physically short cracks are investigated by means of linear elastic fracture mechanics. Therefore the plastic zone ahead of the crack tip must be small in comparison to the crack length. Several fatigue experiments for different notch depths and stress ratios were done on single edge notched bending (SENB) specimens. To investigate the crack growth behaviour in the near-threshold regime, the specimens were pre-cracked in compression [Sur85, Chr86, Hol86, Pip87b, Pip87c, Now87]. To fulfil the conditions of LEFM even for very small notches the applied loads during compression should be as small as possible. To this purpose, specimens were prepared initially a few millimetres higher in width, then a long notch was machined into the specimens and the specimens were compression pre-cracked. Finally, the specimens were machined to the conventional height so that a short notch remains with an incipient crack which fulfils the requirements of LEFM (see Fig. 2.6).

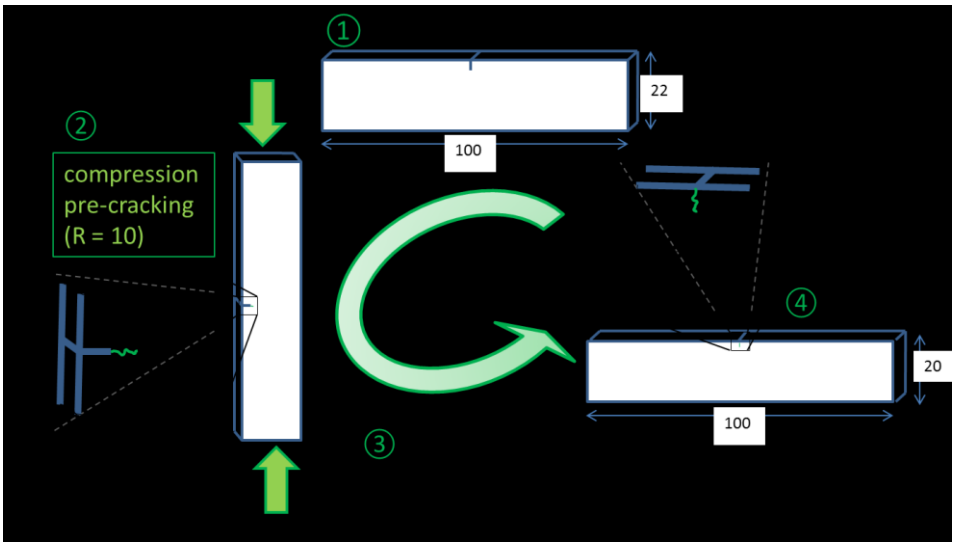

Fig. 2.6 Specimen preparation for short crack growth experiments.

2.2 Mechanical surface treatment processes

There exist various methods for mechanical surface treatment, such as shot peening, laser peening, high frequency impact treatment, deep rolling, et cetera. The effects of such surface treatment processes are mechanical hardening due to cold deformation, mechanical pre-stresses due to residual stresses and reduced or enhanced micro-stress concentrations due to changing surface roughness. In the frame of this work deep rolling and the effect of introduced residual stresses on the crack growth lifetime is considered.

2.2.1 Deep rolling

Deep rolling deforms a component near the surface plastically by pressing discs or spherical tools into the material. The aim of this method is to introduce residual stresses and mechanical hardening in the rolled surface layers to increase in particular the endurance limit [Woh00]. But also the influence on the crack growth rate due to the introduced residual stresses is significant. So the crack growth rate decreases in the presence of compressive residual stresses, but increase in the presence of tensile residual stresses. This is because the residual stresses modify the mean stress during cyclic loading. For compressive residual stresses the mean stress as well as the load ratio R decreases; and the lower the load ratio, the lower is the crack growth rate $\mathrm{d}a/\mathrm{d}N$. It follows that for cyclically loaded components compressive residual stresses near the surface are desirable, whereas tensile residual stresses should be avoided.

To obtain a defined surface treated zone, deep rolling process parameters such as rolling force, number of rolling and feed rate are crucial [Che11]. But also the geometries of the component and the rolling tool are important.

The expected influence of different rolling forces on the hardness and residual stresses is shown in Fig. 2.7. The hardness as well as the compressive residual stresses increase with increasing rolling force (F1-F3), whereby the maximum of both is below the surface. For a further increase of the rolling force (F4, F5) the maximum compressive residual stresses and the maximum hardness is shifted to higher surface distances, but the hardness and the residual stresses on the surface decrease. So if the chosen rolling force is too high, the positive effects

of deep rolling vanish and, even worse, the initial surface hardness as well as the endurance limit decrease whereas the crack growth rate increases due to tensile residual stresses. It is therefore crucial to find the optimum process parameter for the rolling process. This problem is treated in detail in Publication A.

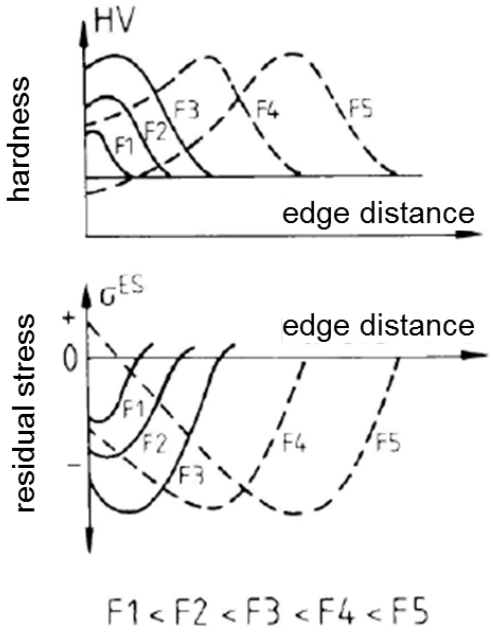

Fig. 2.7 Typical dependence of rolling force on residual stresses and hardness [Ber82].

2.2.2 Stability of residual stresses during operation

If the superposition of residual stresses and load stresses in a component leads to stresses that are higher than the flow stress σ_F, then dislocations can be activated, which leads to a reduction of the residual stresses. Such a reduction of the residual stresses during cyclic loading occurs during the first few load cycles. After at most 1000 load cycles the remaining residual stresses reach a steady state. To predict this remaining residual stress field in a component, a simple analytical model is proposed. This model is based on the assumption that the sum of the remaining residual stresses σ_e and the load stresses σ_b must be smaller or equal than the flow stress R_f:

$$|\sigma_e| + |\sigma_b| \leq R_f \tag{11}$$

Equation (11) implies that if the sum of the initially introduced residual stresses $\sigma_{e,0}$ and the applied load stresses σ_b is higher than the increased flow stress R_f, then the remaining residual stresses σ_e after cyclic loading can be calculated by subtracting the applied load stress from the increased flow stress:

$$|\sigma_{e,0}| + |\sigma_b| > R_f \Rightarrow |\sigma_e| = R_f - |\sigma_b| \tag{12}$$

In contrast, if the sum of the initially introduced residual stresses $\sigma_{e,0}$ and the applied load stresses σ_b is lower than the flow stress R_f, then no reduction of the residual stresses takes place and the remaining residual stresses are equal to the initial residual stresses:

$$|\sigma_{e,0}| + |\sigma_b| \leq R_f \Rightarrow \sigma_e = \sigma_{e,0} \tag{13}$$

In Fig. 2.8 the model prediction is compared with experimentally determined residual stress profiles. Using Eq. (11-13) the remaining residual stress profile (blue curve) can be calculated if the initial residual stress profile (purple curve) and the applied load stress (red curve) are known. The experimentally determined residual stress profile (green curve) shows good agreement with the model prediction.

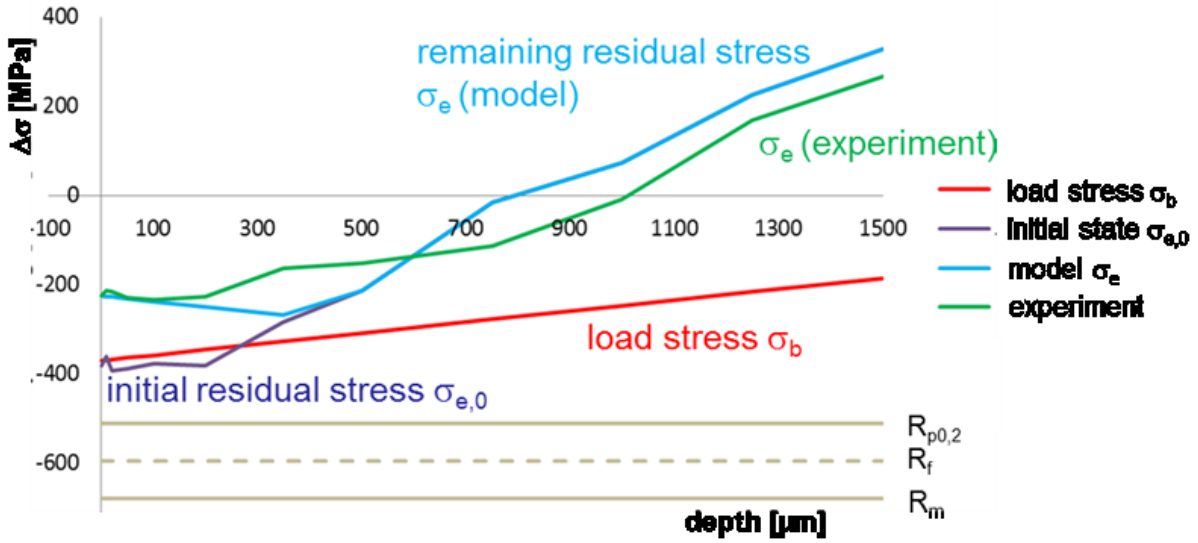

Fig. 2.8 Simple model to predict the reduction of residual stresses during cyclic loading (for details cf. the main text).

2.3 Measurement of residual stresses

There exist various destructive as well as non-destructive methods to determine residual stresses [Sch88, Hau97, Sch97]. Non-destructive methods are, for example, diffraction methods (X-ray, neutron beam); destructive methods are almost all mechanical methods (hole-drilling, cut compliance, contour, et cetera). In this work the cut-compliance method and the X-ray diffraction method were used.

2.3.1 X-ray diffraction method

X-ray diffraction (XRD) is a non-destructive method to determine residual stresses with a high resolution (~0.1 mm) on the surface of a component.

XRD gives the opportunity to determine the lattice parameters of crystalline materials using the Bragg law. The XRD method is based on the measurement of the lattice plane distances as a function of the angle ψ (coordinate system in Fig. 2.9), whereby also lattice planes which are not parallel to the surface give a contribution to the diffraction. The strain measured in the coordinate system (ψ, ϕ) is calculated using Eq. (14) as a function of $\sin^2\psi$.

$$\varepsilon_{\varphi,\psi} = \frac{1+\nu}{E} \cdot \sigma_{\varphi} \sin^2\psi - \frac{\nu}{E} \cdot (\sigma_1 + \sigma_2) \tag{14}$$

This means that the stress can be determined from the slope of the $\varepsilon_{\varphi,\psi}$ vs. $\sin^2\psi$ curve [Cul78, Eig95, Eig96].

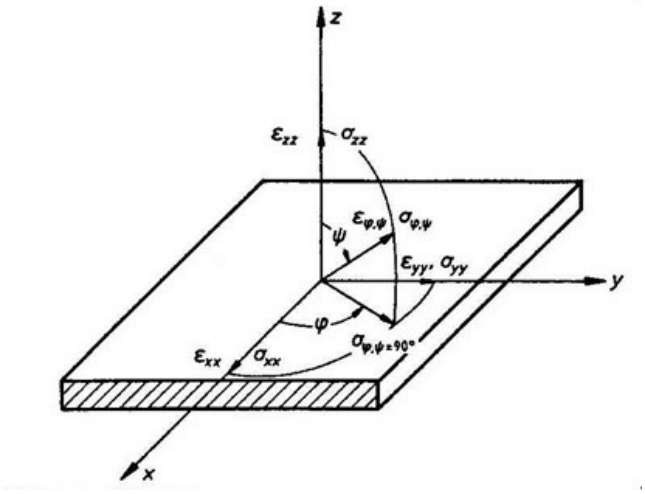

Fig. 2.9 Coordinate system for the XRD stresses measurement.

2.3.2 Cut-Compliance method

The Cut-Compliance (CC) method developed by Cheng and Finnie [Che86, Che94] is a destructive mechanical method to determine residual stresses of a component. The idea of the CC method is to release the residual stresses by introducing progressively a cut into the component. From the change of strain due to this progressive cutting it is possible to calculate the distribution of the released stresses [Sch98]. To measure the change of strain, strain gauges have to be placed on the component (see Fig. 2.10). Using the CC method it is possible to determine the residual stress distribution normal to the cutting surface.

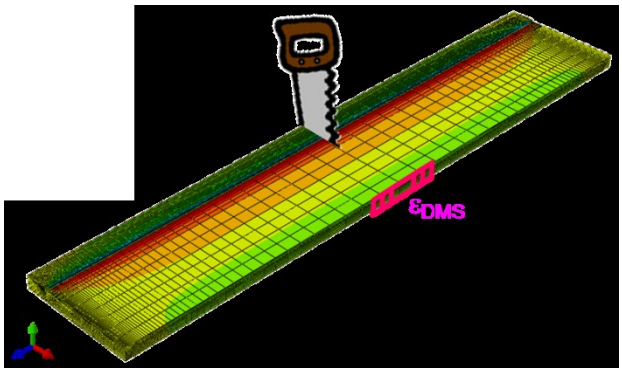

Fig. 2.10 Schematic illustration of the CC method to determine the residual stresses in axial direction (z) of a plate.

In the frame of this work the CC method was verified for a SENB specimen using Finite Element simulations. To this purpose, a residual stress field was introduced in a specimen by plane compression. Afterwards the specimen was cut with successive cutting increments of 1 mm, and the released strains $\Delta\varepsilon_{DMS}$ were measured at the edge of the specimen (Fig. 2.10, Fig. 2.11).

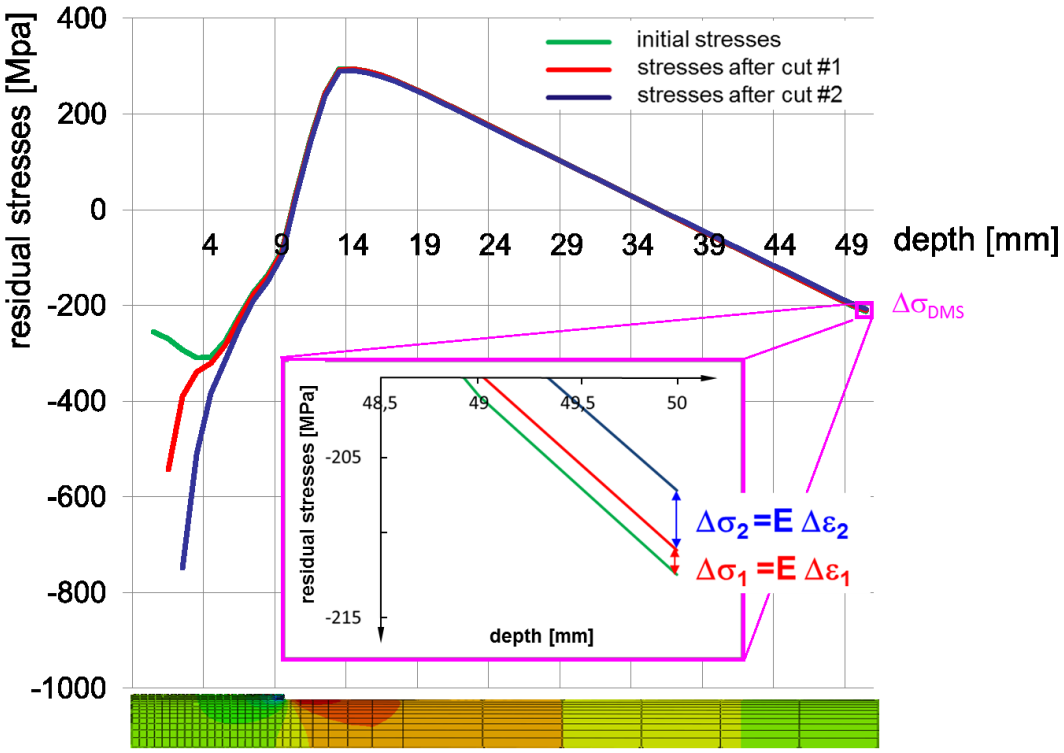

Fig. 2.11 Rearrangement of residual stresses for the first two cutting steps.

If, from an actual experiment, only the $\Delta\varepsilon_{DMS}$ are known, the initial stress distribution is calculated via the procedure described in what follows. This method was used for the experiments in Publication C.

From the strain change $d\varepsilon_{DMS}$ with the increase of cutting depth da, the stress intensity factor K_{Irs} depending from the residual stresses can be calculated from

$$K_{Irs}(a) = \frac{E}{Z(a)} \cdot \frac{d\varepsilon_M}{da} \quad , \tag{15}$$

where E is Young's modulus and $Z(a)$ a geometry-dependent influence function.

Subsequently the initial residual stress distribution can be calculated using

$$K_{Irs}(a_i) = \sigma_0 \cdot \int_0^{a_0} h(x,a_i)\cdot dx + \sum_{j=1}^{i-1} \sigma_j \cdot \int_{a_{j-1}}^{a_j} h(x,a_i)\cdot dx + \sigma_i \cdot \int_{a_{i-1}}^{a_i} h(x,a_i)\cdot dx \tag{16}$$

where, again, $h(x, a_i)$ is a geometry-dependent influence function [Sch97]. Due to the layer removal a homogeneous residual stress distribution over the specimen thickness is required. If the residual stress changes over the thickness, then the CC method provides an averaged residual stress. That implies that this method does not consider potentially occurring stress gradients over the thickness.

2.4 Fracture control concepts

The three major fracture control concepts are (i) the safe-life concept, (ii) the fail-safe concept, and (iii) the damage tolerance concept [Sur98, San08].

(i) The safe-life concept implies that a component must be designed in a way that it will not fail during service life. To verify whether a component is safe for a certain amount of load cycles, stress-life (S/N) curves are used in most cases.

(ii) In contrast the fail-safe concept allows local cracks if final fracture can be excluded. With a Kitagawa-Takahashi (KT) diagram it is possible, for any given crack length and stress range, to assess whether a component under these conditions leads to finite life or if the component is still rated for endurance (infinite lifetime). The KT diagram is a broadly used tool which combines the endurance limit with the fatigue crack propagation threshold in one diagram. Thereby it defines areas of finite as well as of infinite life.

(iii) Finally, in the damage tolerance concept fatigue crack extension is basically accepted. The aim is to prevent the crack to grow to its critical size during total lifetime or during an inspection interval. To this purpose it is essential to describe the crack growth rate as accurate as possible.

For all three fracture control concepts the lifetime of a component can be increased significantly by introducing compressive residual stresses by means of surface treatment methods. The endurance limit will be higher than in untreated components (safe-life), also crack arrest occurs over a larger crack extension length due to the increased threshold for crack propagation (fail-safe), and finally the crack growth rate also decreases in the presence of residual stresses due to the reduced mean stress (damage tolerance).

3 Summary

In order to increase the fatigue lifetime or to reduce the number of inspection intervals, deep rolling provides a simple way to prevent crack growth emanating whether from the smooth surface of a component or from defects. To know up to which depth the compressive residual stresses persist, semi-empirical formulas were derived in the course of this thesis using finite element simulations of several deep rolling tools with different geometries as well as experimentally determined stress distributions from deep rolled specimens and drivetrain components (Publication A). The results of these investigations show that the depth of the residual stresses depends only on the geometry of the Hertzian contact ellipse. For cyclically loaded components the question about the stability of the introduced compressive residual stresses during operation arises. Therefore the initial residual stress distributions of surface treated specimens were compared with the stress distributions after a certain amount of load cycles. The investigations show that for high loads of 500 MPa the compressive residual stresses are reduced within the first few load cycles. It turned out that deep rolling is a simple and effective process to prevent (or at least to significantly slow down) crack growth and thereby to increase the lifetime or reduce the number of inspection intervals in cyclically loaded components.

Furthermore also an accurate model to describe the crack growth behaviour of cracks of arbitrary length is essential for the damage tolerance assessment of a cyclically loaded component. In this thesis, the fatigue crack growth behaviour of short and long cracks in the quenched and tempered steel 25CrMo4 was investigated experimentally. To this purpose, Single Edge Notched Bending (SENB) specimens with different notch depths were machined. The specimens were compression pre-cracked to obtain a fatigue pre-crack, and subsequently subjected to cyclic loading under eight-point bending. The experiments were conducted under step-wise increasing constant loads and the crack growth rate was monitored in detail. For short crack extension the crack grows initially below the threshold for long cracks, but due to the build-up of crack closure crack arrest occurs eventually (Publication B). Based on the experimental results, an analytical fatigue crack growth model for the build-up of crack closure effects during crack extension was developed. This analytical model for the build-up of crack closure was integrated into the conventional NASGRO equation (Publication B). This modified NASGRO equation is now able to describe the crack growth rate for cracks of

arbitrary length. In Fig. 3.1 the prediction of the modified NASGRO equation is compared to experimental results, showing good agreement.

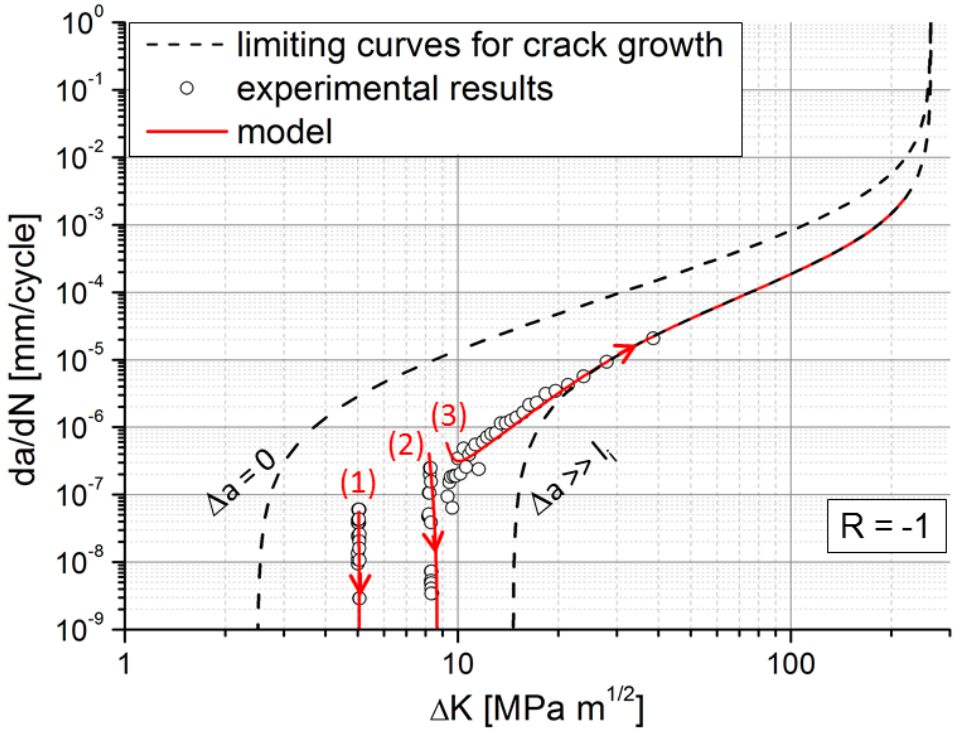

Fig. 3.1 Growth of a short crack near the threshold region – comparison of experiment and prediction.

With this model it is possible to predict fatigue lifetime or necessary inspection intervals more accurately in the context of damage tolerant design and fitness-for-purpose assessments.

The combined influence of the build-up of crack closure during crack propagation and compressive residual stresses on the crack growth rate is investigated in Publication C. To investigate the crack growth in the presence of residual stresses, specimens with a special geometry were developed. In those specimens extended areas of tensile as well as compressive residual stresses were introduced by means of rolling. During rolling, the specimen is deformed plastically below the areas of contact, thus a residual stress field is generated that varies from high compressive residual stresses at the edges to lower tensile residual stresses in the middle of the specimen. Afterwards again fatigue experiments were done using the eight-point-bending method and step-wise increasing constant load tests. The results of the experiments show a significant decrease of the crack propagation rate; also crack arrest occurs in the rolled specimen at stress intensities which are higher than the long crack threshold in residual stress free specimens. The determined long crack threshold was approximately 4.5 times higher than in a residual stress free specimen (Publication C). To

consider a residual stress field in the modified NASGRO equation, the minimum and maximum local stresses during one load cycle were calculated by superposition of cyclic load stresses and residual stresses. With the minimum and maximum local stresses the minimum and maximum crack tip loading can be estimated using an influence function. Finally, the stress ratio and the stress intensity factor range can be calculated and used in the modified NASGRO equation to predict the crack growth rate in the presence of residual stresses.

To estimate the endurance limit of components with an already existing flaw, the Kitagawa-Takahashi diagram allows to predict, for cracks of given length, the allowable stress range for infinite life. But, as shown in Publication D, caution is advised if a crack emanates not directly from the plane surface but from a sharp, crack-like notch instead. In this thesis, the influence of the initial flaw size was studied by different notch depths. Experiments showed that, the deeper the initial notch compared to the total crack length, the lower is the resistance against crack propagation. It was shown that it depends on both portions of a crack, namely the notch depth and the crack extension, whether a cracked component exhibits finite or infinite fatigue lifetime at a given stress amplitude. Based on the splitting of the total crack length into the notch depth and the real crack extension length, and the build-up of crack closure during crack extension, an enhanced Kitagawa-Takahashi (KT) diagram was proposed (Publication D). In this enhanced KT diagram the threshold stress range is plotted against the crack extension and the initial notch depth, respectively. The modified KT diagram shows good agreement with experimental data, see Fig. 3.2.

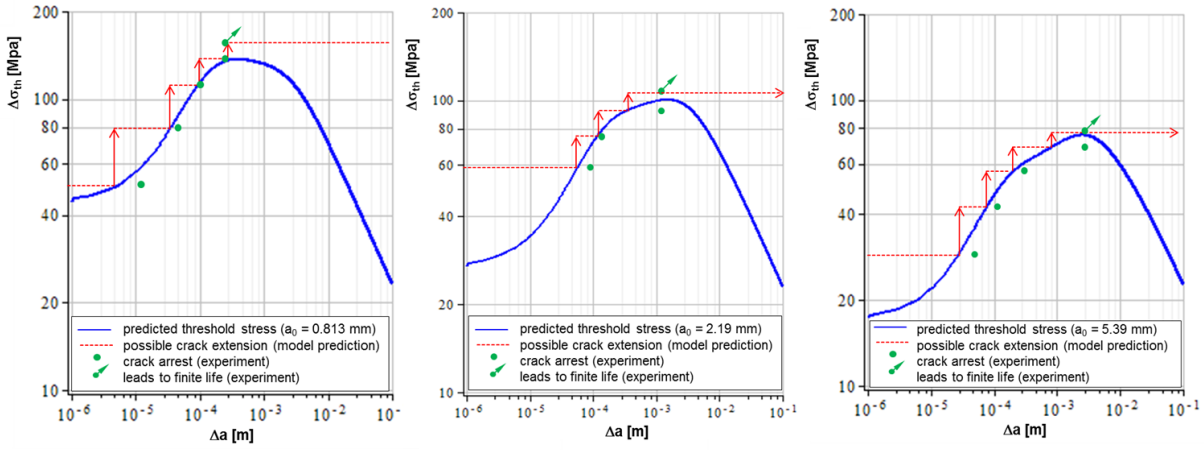

Fig. 3.2 Comparison of the predicted crack extension with experimental results for samples with different notch depths.

With the results of this thesis, it will therefore be possible, in the context of damage tolerant design, to predict fatigue lifetime or necessary inspection intervals for components containing residual stresses and small flaws more accurately.

Bibliography

[And05] Anderson TL. Fracture Mechanics: Fundamentals and Applications. 3rd ed, CRC Press, 2005.

[Ber82] Berstein G, Fuchsbauer B. Festwalzen und Schwingfestigkeit. Materialwissenschaft und Werkstofftechnik 13, 1982, 103-109.

[Che86] Cheng W, Finnie I. Measurement of Residual Hoop Stresses in Cylinders Using the Compliance Method. ASME Journal of Engineering Materials and Technology, 108, 1986, 87-92.

[Che94] Cheng W, Finie I. An Overview of the Crack Compliance Method For Residual Stress Measurement. 4th International Conference On Residual Stresses, Baltimore, 1994, 449-458.

[Che11] Cherif A. Analyse und Beurteilung gekoppelter thermisch-mechanischer Prozesse zur Randschichtverfestigung. Forschungsbericht aus dem Institut für Werkstofftechnik-Metallische Werkstoffe der Universität Kassel, Band 12, 2011.

[Chr86] Christman T, Suresh S. Crack initiation under far-field cyclic compression and the study of short fatigue cracks. Engineering Fracture Mechanics 23, 1986, 953-964.

[Cul78] Cullity BD. Elements of X-ray Diffraction. Addison-Wesley Publishing Company Inc, Second Edition, 1978.

[Eig95] Eigenmann B, Macherauch E. Röntgenografische Untersuchung von Spannungszuständen in Werkstoffen: Teil II. Materialwissenschaften und Werkstofftechnik 26, 1995, 199-216.

[Eig96] Eigenmann B, Macherauch E. Röntgenografische Untersuchung von Spannungszuständen in Werkstoffen: Teil III. Materialwissenschaften und Werkstofftechnik 27, 1996, 426-437.

[Elb70] Elber W. Fatigue Crack Closure under Cyclic Tension. Engineering Fracture Mechanics, Vol 2, 1970, 37-45.

[Fet08] Fett T. Stress Intensity Factors – T-Stresses – Weight Functions. Universitätsverlag Karlsruhe, 2008.

[For62] Forman RG, Keary VE, Engle RM. Numerical Analysis of Crack Propagation in Cyclic-Loaded Structures. Journal of Basic Engineering, Vol 89, 1967, 459-464.

[For92] Forman RG, Mettu SR. Behavior of Surface and Corner Cracks Subjected to Tensile and Bending Loads in Ti-6Al-4V Alloy. ASTM STP 1131, American Society for Testing and Materials, Philadelphia, PA, 1992, 519-546.

[Fro56] Frost NE, Phillips CE. Studies in the formation and propagation of cracks in fatigue specimens. Proc Int Conference on Fatigue of Metals, London, 1956.

[Gri20] Griffith AA. The Phenomena of Rupture and Flow in Solids. Philosophical Transactions, Series A, Vol. 221, 1920, 163-198.

[Gro07] Gross D, Seelig T. Bruchmechanik: Mit einer Einführung in die Mikromechanik. 4te Auflage, Springer, 2007.

[Hau97] Hauk V. Structural and Residual Stress Analysis by Nondestructive Methods. Elsevier, Amsterdam, 1997.

[Hol86] Holm DK, Blom AF, Suresh S. Growth of cracks under far-field cyclic compression loads: numerical and experimental results. Engineering Fracture Mechanics 23, 1986, 1097-1106.

[Irw57] Irwin GR. Analysis of stresses and strains near the end of a crack traversing a plate. Journal Applied Mechanics, Vol 25, 1957, 361-364.

[Kit90] Kitagawa H, Tanaka T. Applicability of fracture mechanics to very small cracks or the cracks in the early stage. Proceedings of Second International Conference on Mechanical Behavior of Materials, 1990, 627-631.

[Kle72] Klesnil M, Lukas P. Influence of Strength and Stress History on Growth and Stabilisation of Fatigue Cracks. Engineering Fracture Mechanics, Vol 4, 1972, 77-92.

[Lan82] Lankford J. The growth of small fatigue cracks in 7056-T6 aluminium. Fatigue of Engineering Materials and Structures 5, 1982, 233-248.

[McE88] McEvily AJ. On Closure in Fatigue Crack Growth. ASTM STP 982, American Society for Testing and Materials. Philadelphia, PA, 1988, 35-43.

[Mil86] Miller KJ, de los Rios ER. Editors, The Behaviour of Short Fatigue Cracks. London: Mechanical Engineering Publications, 1986.

[Mur87] Murakami Y. Stress intensity factors handbook. Pergamon press, 1987.

[New84] Newman JC. A crack opening stress equation for fatigue crack growth. Int J Fract 24, 1984, R131-R135.

[New99] Newman JC, Phillips EP, Swain MH. Fatigue-life prediction methodology using small-crack theory. Int J Fatigue, Vol 21, Issue 2, 1999, 109-119.

[Now87] Nowack H, Marissen R. Fatigue crack propagation of short and long cracks: physical basis, prediction methods and engineering significance. Proc Fatigue 87 (Edited by Richtie RO and Starke EA), EMAS, Warley, UK, 1987, 207-230.

[Par61] Paris PC, Gomez MP, Anderson WP. A rational analytic theory of fatigue. The Trends in Engineering 13, 1961, 9-14.

[Par63] Paris PC, Erdogan F. A critical analysis of crack propagation laws. Journal of Basic Engineering 85, 1963, 528-534.

[Pea75] Pearson S. Initiation of fatigue cracks in commercial aluminium alloys and the subsequent propagation of very short cracks. Engineering Fracture Mechanics 7, 1975, 235-247.

[Pip87a] Pippan R, Berger M, Stüwe HP. The influence of crack length on fatigue crack growth in deep sharp notches. Metall Trans 18A, 1987, 429-435.

[Pip87b] Pippan R. The growth of short crack under cyclic compression. Fatigue Fracture Engineering Materials 90, 1987, 319-328.

[Pip87c] Pippan R. Threshold and crack-growth tests on pre-cracked specimens produced in cyclic compression. Proc Fatigue 87 (Edited by Richtie RO and Starke EA), EMAS, Warley, UK, 1987, 933-940.

[Pip11] Pippan R. Ausgewählte Kapitel der Festkörpermechanik (Bruchmechanik). Lecture notes, winter semester 2011/12.

[Rad07] Radaj D, Vormwald M. Ermüdungsfestigkeit: Grundlagen für Ingenieure (German Edition), Springer, 2007.

[Rit80] Ritchie RO, Suresh S, Moss CM. Near-threshold fatigue crack growth in $2\frac{1}{4}$ Cr-1 Mo pressure vessel steel in air and hydrogen. Journal of Engineering Materials and Technology 102, 1980, 293-299.

[Rit86] Ritchie RO, Lankford J. Editors, Small Fatigue Cracks. Warrendale: The Metallurgical Society of the American Institute of Mining, Metallurgical and Petroleum Engineers, 1986.

[San08] Sander M. Sicherheit und Betriebsfestigkeit von Maschinen und Anlagen: Konzepte und Methoden zur Lebensdauervorhersage. Springer, 2008.

[Sch88] Schajer GS. Measurement of nun-uniform residual stresses using the hole drilling method – part I: Stress calculation procedure. Journal of Engineering Materials and Technology, Transactions of the ASME, Vol 110, 1988, 338-343.

[Sch09] Schijve J. Fatigue of Structures and Materials. 2nd ed, Springer, 2009.

[Sch97] Schindler HJ, Bertschinger P. Some Steps Towards Automation of the Crack Compliance Method to Measure Residual Stress Distributions, In: Proceedings 5th International Conference on Residual Stress, Linköping, 1997.

[Sch98] Schindler HJ. Experimental Determination of Crack Closure by the Cut Compliance Technique. Advances in Fatigue Crack Closure Measurement and Analysis, ASTM STP 1343, RC McClung and JC Newman Jr, Editors, American Society for Testing and Materials, 1998.

[Sur81] Suresh S, Zamiski GF, Ritchie RO. Oxide-induced crack closure: an explanation for near-threshold corrosion fatigue crack growth behaviour. Metallurgical Transactions 10A, 1981, 1435-1443.

[Sur82] Suresh S, Ritchie RO. A geometric model for fatigue crack closure induced by fracture surface morphology. Metallurgical Transactions 13A, 1982, 1627-1631.

[Sur84a] Suresh S, Ritchie RO. Propagation of short fatigue cracks. International Metals Review 29, 1984, 445-476.

[Sur84b] Suresh S, Ritchie RO. Near-threshold fatigue crack propagation: a perspective on the role of crack closure. In Fatigue Crack Growth Threshold Concepts (eds Davidson DL & Suresh S), Warrendale: The Metallurgical Society of the American Institute of Mining, Mineral and Petroleum Engineers, 1984, 227-261.

[Sur85] Suresh S. Crack initiation in cyclic compression and its applications. Engineering Fracture Mechanics 21, 1985, 453-463.

[Sur98] Suresh S. Fatigue of Materials. Cambridge University Press. 2nd ed, Cambridge 1998.

[Tad00] Tada H, Paris P, Irwin G. The stress analysis of cracks handbook. 3rd ed, The Amercian Society of Mechanical Engineers, 2000.

[Tan83] Tanaka K, Nakai Y. Propagation and Non-Propagation of Short Fatgiue Cracks at a Sharp Notch. Fatigue of Engineering Materials and Structures, Vol 6, 1983, 315-327.

[Woh00] Wohlfahrt H, Krull P. Mechanische Oberflächenbehandlungen: Grundlagen-Bauteileigenschaften-Anwendungen. Wiley-Vch Verlag GmbH, 2000.

[Wu91] Wu XR, Carlsson AJ. Weight Functions and Stress Intensity Factor Solutions. Pergamon press, 1991.

List of appended publications & proceedings

[A] J. Maierhofer, H.-P. Gänser, R. Pippan. Prozessmodell zum Einbringen von Eigenspannungen durch Festwalzen. Submitted.

[B] J. Maierhofer, R. Pippan, H.-P. Gänser. Modified NASGRO equation for physically short cracks. International Journal of Fatigue 59 (2014), 200-207.

[C] J. Maierhofer, R. Pippan, H.-P. Gänser. Modified NASGRO equation for short cracks and application to the fitness-for-purpose assessment of surface-treated components. Procedia Materials Sciene, 20th European Conference on Fracture (ECF20, accepted).

[D] J. Maierhofer, H.-P. Gänser, R. Pippan. Modified Kitagawa-Takahashi diagram – a practical modelling approach. Submitted.

Publication A: Prozessmodell zum Einbringen von Eigenspannungen durch Festwalzen

Prozessmodell zum Einbringen von Eigenspannungen durch Festwalzen

J. Maierhofer*, H.-P. Gänser[1], R. Pippan[2]

* Jürgen Maierhofer, Materials Center Leoben Forschung GmbH, Roseggerstraße 12, A-8700 Leoben; juergen.maierhofer@mcl.at; Fax +43 384245922-5

[1] Hans-Peter Gänser, Materials Center Leoben Forschung GmbH, Roseggerstraße 12, A-8700 Leoben

[2] Reinhard Pippan, Erich Schmid Institute of Materials Science, Jahnstraße 12,A-8700 Leoben

Kurzfassung

Defekte an Wellen führen zu einer deutlichen Reduktion der Lebensdauer. Festwalzen bietet eine einfache Möglichkeit, Risswachstum an Defekten zu verlangsamen oder überhaupt zu verhindern, vorausgesetzt die Fehlergröße überschreitet nicht die Einflusszone der eingebrachten Druckeigenspannungen. Im Rahmen dieser Arbeit wird ein einfaches Prozessmodell vorgestellt mit welchem es möglich ist, die Eindringtiefe von Druckeigenspannungen abzuschätzen.

Einleitung

Ein kürzlich erschienener Überblick [1] über Betriebsfestigkeit und Schadenstoleranz von Radsatzwellen weist unter anderem auf die Bildung von Ermüdungsrissen an Korrosionsgrübchen, Steinschlägen (welche auf Hochgeschwindigkeitsstrecken erhöht auftreten) und an nichtmetallischen Einschlüssen hin. An Gegenmaßnahmen wird neben Beschichtungen zur Vermeidung von Korrosion und Steinschlag auf eine Erhöhung der metallurgischen Reinheit wie Elektroschlacke-Umschmelzen sowie auf Wärmebehandlungen und Festwalzen zum Einbringen von Druckeigenspannungen verwiesen.
Im vorliegenden Beitrag wird näher auf das Festwalzen und seine Auswirkungen auf die Schadenstoleranz eingegangen. Insbesondere werden einige einfache Faustformeln abgeleitet, um in Abhängigkeit der Geometrie von Werkstück und Werkzeug die notwendigen Festwalzkräfte und die daraus resultierenden Eigenspannungsfelder abzuschätzen. Darüber hinaus werden Aussagen über die Stabilität der Eigenspannungen getroffen. Dies gestattet in weiterer Folge, den Einfluss dieser Eigenspannungen auf die Wachstumsfähigkeit möglicherweise vorhandener Ermüdungsrisse abzuschätzen. Somit kann bereits in frühen Phasen der Auslegung mit geringem Aufwand beurteilt werden, ob eine Oberflächenbehandlung durch Festwalzen notwendig und zielführend erscheint.

Problemstellung, Ziel und Ablauf der Untersuchungen

Es existieren eine Reihe unterschiedlicher Werkzeuge zum Festwalzen von Radsatzwellen. Diese Werkzeuge werden mit deutlich unterschiedlichen Anpresskräften beaufschlagt, um die gewünschte Wirkung zu erzielen; die Ermittlung der optimalen Anpresskräfte erfolgt üblicherweise in aufwändigen Versuchsreihen. Mit dem Ziel der Bestimmung des Einflusses des Festwalzwerkzeuges auf die resultierenden Eigenspannungen wurden Radsatzwellen mit zwei verschiedenen Werkzeugen A und B nach dem Vorschubverfahren festgewalzt und anschließend die Eigenspannungsverläufe bestimmt. Ergänzt wurde diese Versuchsreihe durch Literaturdaten aus dem Projekt MARAXIL [2] (d_1 = 85 mm, r_3 =2,5 mm). Zusätzlich wurden Laborproben kleiner Abmessungen festgewalzt, um den Eigenspannungsabbau unter Betriebsbeanspruchung zu quantifizieren. Im Vergleich zum Projekt MARAXIL weisen die

Festwalzrollen A und B deutlich größere Durchmesser d_1 und Rundungsradien r_3 auf, sodass insgesamt ein breiter Bereich möglicher Werkzeuggestaltungen abgedeckt wird.

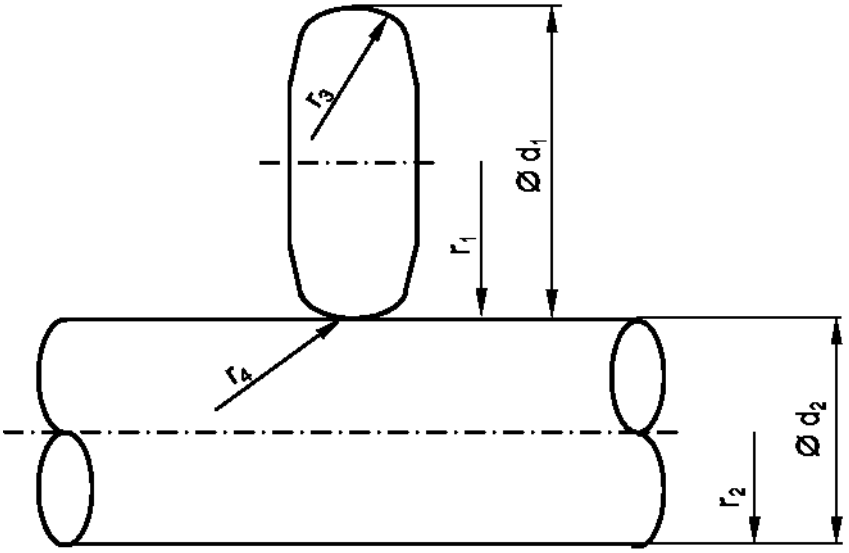

Abb. A.1: Festwalzen von Wellen nach dem Vorschubverfahren; d_1 Durchmesser der Festwalzrolle, r_1 Radius der Festwalzrolle, d_2 Wellendurchmesser, r_2 Wellenradius, r_3 axialer Krümmungsradius der Festwalzrolle, r_4 axialer Krümmungsradius der Welle ($\rightarrow\infty$ bei zylindrischen Wellen).

Für die experimentellen Versuche wurde der Vergütungsstahl 25CrMo4 gewählt, welcher typischerweise als Material für Eisenbahnwellen verwendet wird. Dieser Stahl hat eine bainitische Mikrostruktur und ein Härte von ~ 245 HV. Die im Zugversuch ermittelte Fließgrenze liegt bei 512 MPa, die Zugfestigkeit beträgt 674 MPa bei einer Bruchdehnung von 18.9%.

Einbringen von Eigenspannungen durch Festwalzen – Versuch und Modellbildung

Beim Festwalzen werden Eigenspannungen durch die plastische Verformung der oberflächennahen Werkstoffschicht hervorgerufen: das plastische Eindrücken in radialer Richtung bewirkt bleibende plastische Dehnungen in Längs- und Umfangsrichtung; diese Dehnungen werden durch elastische Stauchung in Längs- und Umfangsrichtung kompensiert, wodurch Druckspannungen an der Oberfläche entstehen.

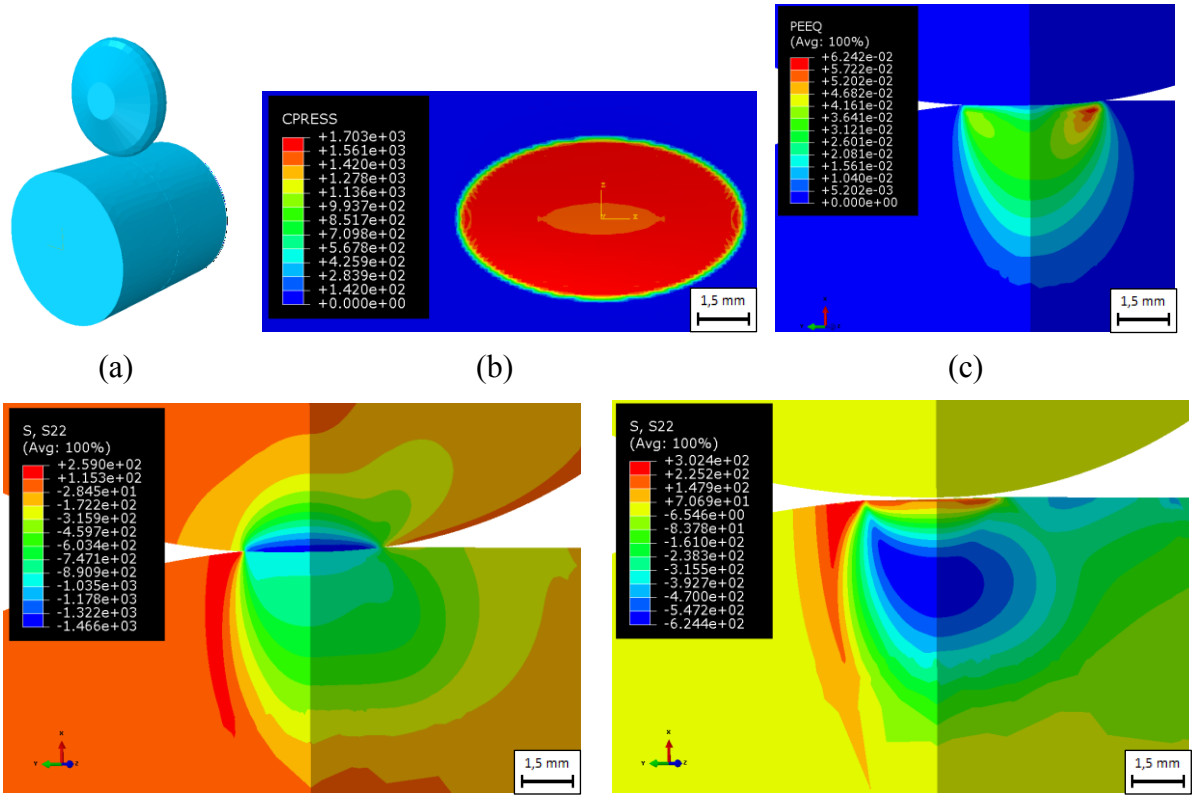

Abb. A.2: Finite-Elemente-Simulationen des Werkzeugkontakts – Radsatzwelle mit Werkzeug A; (a) Finite-Elemente Modell, (b) Kontaktbereich, (c) plastische Zone, (d) Axialspannungen während des Anpressens des Werkzeuges, (e) Axialspannungen nach Entfernen des Werkzeuges.

Abb. A.2 zeigt die Verformungs- und Spannungsfelder, welche durch das radiale Anpressen des Werkzeuges an das Werkstück entstehen, vorerst ohne Werkzeugbewegung in Umfangs- und Längsrichtung. Das Finite-Elemente-Modell für das Anpressen des Werkzeuges A an

eine Radsatzwelle aus 25CrMo4 mit 190 mm Durchmesser ist in Abb. A.2a dargestellt. Es stellt sich ein ellipsenförmiger Kontaktbereich mit fast konstanter Flächenpressung ein (Abb. A.2b). Darunter bildet sich eine plastische Zone aus, welche bis in eine Tiefe t_p reicht (Abb. A.2c). Während des Anpressens entstehen Spannungen in Längsrichtung der Welle (Abb. A.2d), welche sich in der Nähe der Oberfläche beim Entfernen des Werkzeugs noch etwas umlagern und so schließlich die Eigenspannungen ergeben (Abb. A.2e).

Die numerische Simulation des Anpressens ergibt direkt an der Oberfläche Zugeigenspannungen in Längsrichtung, welche erst etwas unterhalb der Oberfläche in Druckspannungen mit einer Reichweite von t_s in die Tiefe umschlagen. Durch die Rotation des Werkstücks beim Festwalzen stellt sich dieser Verlauf gleichermaßen entlang des gesamten Werkstückumfangs ein.

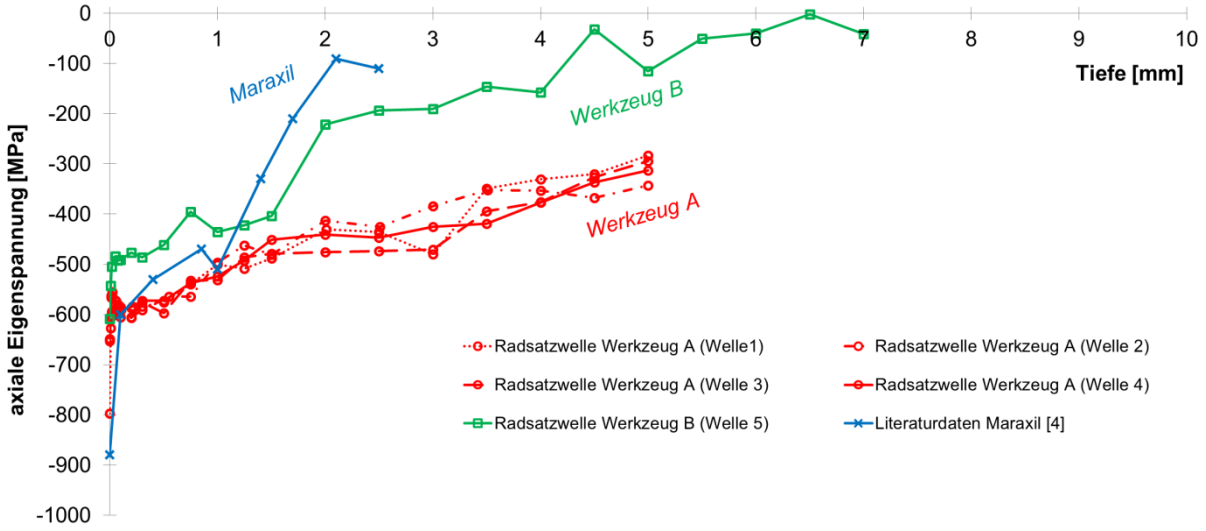

Abb. A.3: Experimentell bestimmte Eigenspannungen in festgewalzten Radsatzwellen.

In Abb. A.3 sind die an Radsatzwellen ermittelten Eigenspannungsverläufe, welche mit unterschiedlichen Werkzeugen eingebracht wurden, dargestellt. Im Gegensatz zur Simulation werden im Experiment direkt an der Oberfläche bereits Druckeigenspannungen beobachtet; der Grund dafür ist in einer weiteren Spannungsumlagerung aufgrund der zyklischen Plastizierung beim mehrfachen Überrollen zu sehen. Die Höhe der Druckeigenspannungen an der Oberfläche liegt bei allen untersuchten Werkzeuggeometrien im Bereich der Fließgrenze.

Während eine detaillierte numerische Simulation des Festwalzvorganges mit mehrfachem Überrollen und genauer Berücksichtigung des zyklischen Verfestigungsverhaltens inzwischen – wenngleich unter hohem Rechenaufwand – möglich ist und z.B. im Forschungsprojekt

MARAXIL durchgeführt wurde, soll an dieser Stelle ein einfacherer Zugang gewählt werden, der sich für erste überschlägige Abschätzungen und den Vergleich verschiedener Festwalzwerkzeuge besser eignet.

Dazu fassen wir die soeben beschriebenen Beobachtungen in einem vereinfachten Prozessmodell nach dem Schema in Abb. A.4 wie folgt zusammen:

- Zwischen Werkzeug und Werkstück bildet sich eine annähernd elliptische Kontaktfläche; in dieser Kontaktfläche herrscht eine weitestgehend konstante Flächenpressung vom ungefähr Dreifachen der Streckgrenze (Abb. 2b).
- Die hohen Kontaktspannungen führen zu einer plastischen Verformung bis in eine Tiefe t_p („Eindringtiefe der plastischen Verformung“).
- Die plastische Verformung führt zu Druckeigenspannungen, welche an der Oberfläche in Längsrichtung die Größenordnung der Fließgrenze erreichen (Abb. 3).
- Diese Eigenspannungen gehen in grober Näherung mit zunehmendem Oberflächenabstand in die Tiefe linear zurück (Abb. A.3) und erreichen den Wert Null bei einer Tiefe t_s („Eindringtiefe der Druckeigenspannungen“, schematisch in Abb. A.4).

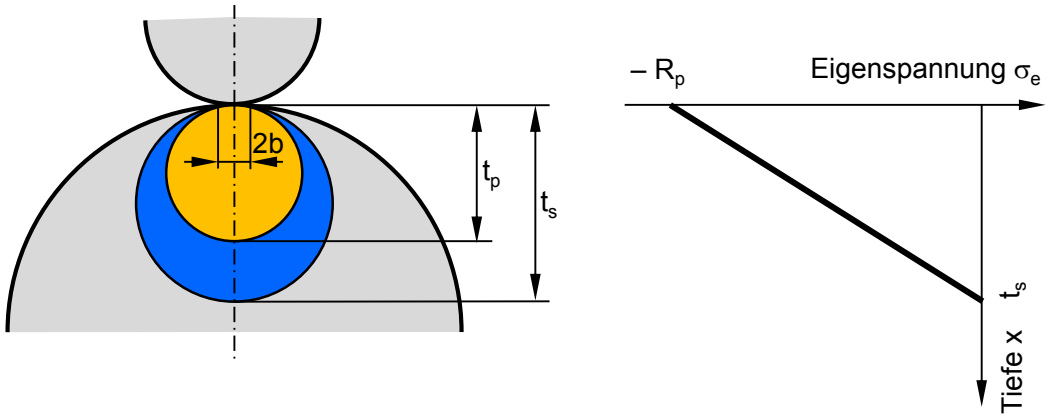

Abb. A.4: Prozessmodell für das Einbringen von Eigenspannungen (schematisch).

Zur vollständigen quantitativen Festlegung des Modells sind nun noch die Eindringtiefen t_p und t_s zu bestimmen. Aufgrund von Ähnlichkeitsüberlegungen kann erwartet werden, dass diese Eindringtiefen proportional zueinander und zum kleinen Halbmesser der Kontaktellipse (Kontakthalbbreite) b sind. Zur groben Abschätzung der Kontakthalbbreite unter Berücksichtigung der Anpresskraft und der Krümmungen der Kontaktkörper eignet sich die Hertzsche Theorie. Aufgrund der Annahme rein elastischen und damit im Vergleich zum tatsächlichen elastoplastischen Kontakt zu steifen Verhaltens wird allerdings im Hertzschen

Kontakt bei gleicher Anpresskraft die mittlere Flächenpressung deutlich über- und die Kontakthalbbreite deutlich unterschätzt (vgl. Werte von FE-Simulation und Hertzscher Lösung in Tab. A.1).

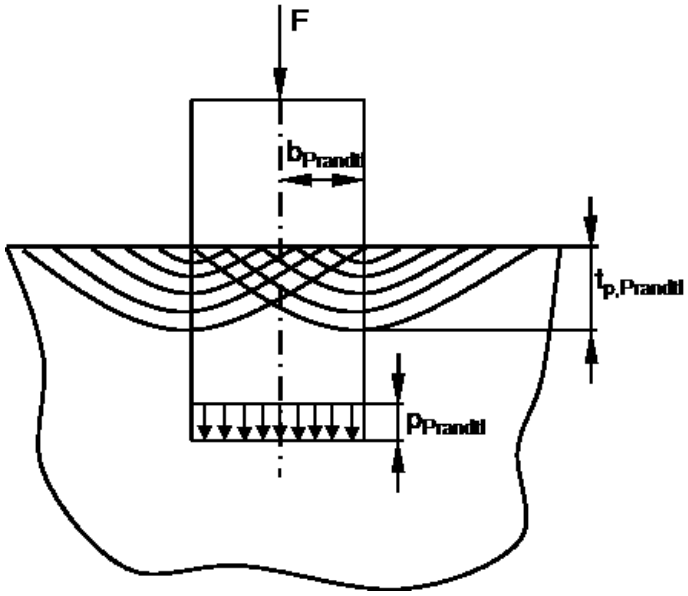

Abb. A.5: Eindrücken eines Flachstempels in einen starr-idealplastischen Halbraum.

Größe	FEM	Hertz	Prandtl	Messung
Anpresskraft F	1	1	1	1
mittlere Flächenpressung p_m	1	2,13±0,37	0,98±0,08	-
Kontakthalbbreite b	1	0,67±0,09	0,97±0,08	-
Eindringtiefe der plastischen Zone t_p	1	-	0,67±0,08	-
Eindringtiefe der Eigenspannungen t_s	1	-	-	1,02±0,29

Tab. A.1: Normierte Größen des Prozessmodells (Mittelwert ± Standardabweichung); auf die Ergebnisse der Finite-Elemente-Simulationen (FEM) bezogene Werte; statistische Auswertung über verschiedene Festwalzpaarungen.

Hingegen zeigt die Prandtlsche Lösung [3, 4, 5] für das Eindringen eines Flachstempels der Breite $2b_{Prandtl}$ in einen starr-idealplastischen Halbraum (Abb. A.5) eine bemerkenswert gute Übereinstimmung mit der Flächenpressung aus den FE-Simulationen. Aufgrund der im Vergleich zur Hertzschen Theorie nun kleineren Flächenpressung bei der Prandtlschen Lösung muss, unter der Annahme von geometrisch ähnlichen Kontaktellipsen, die Kontakthalbbreite b größer sein als bei der Hertzschen Lösung.

Die Kontakthalbbreite für die Prandtlsche Lösung ist aufgrund des nichtkonformen Kontakts nicht von vornherein bestimmt; sie kann aber unter der Annahme, dass die Halbachsen der

Kontaktellipse das selbe Verhältnis haben wie bei der Hertzschen Lösung, aus der mittleren Pressung (1) bei gegebener Festwalzkraft abgeschätzt werden. Diese aus der Prandtlschen Lösung abgeschätzte Kontakthalbbreite zeigt ebenso wie die Flächenpressung eine gute Übereinstimmung mit den FE-Simulationen (siehe Tab. A.1). In Tab. A.1 sind die maßgeblichen Größen des Kontaktproblems bezogen auf die Ergebnisse der FE-Simulation zusammengefasst. Zur Erstellung von Tab. A.1 wurden alle Festwalzpaarungen bewertet, sodass zu jeder Größe sowohl der Mittelwert als auch die empirische Standardabweichung über alle Geometrien angegeben werden kann.

Das Prandtlsche Gleitlinienfeld gestattet nun die Tiefe der plastischen Zone t_p analytisch abzuschätzen. Die entsprechenden Beziehungen lauten

$$p_\mathrm{Prandtl} = 2{,}97 \cdot \sigma_\mathrm{F}\,, \tag{1}$$

$$t_\mathrm{p,Prandtl} = 1{,}414 \cdot b_\mathrm{Prandtl}\,, \tag{2}$$

wobei für die Fließspannung σ_F die 0,2%-Dehngrenze $R_\mathrm{p0,2}$ verwendet werden kann.

Die Kontakthalbbreite der Hertzschen Lösung lässt sich an Hand von Tab. A.1 mit

$$b_\mathrm{Hertz} \approx (0{,}69 \pm 0{,}11) \cdot b_\mathrm{Prandtl} \tag{3}$$

aus der Prandtlschen Lösung abschätzen.

Die Eindringtiefe der Druckeigenspannungen t_s wird schließlich als proportional zu t_p angenommen. Der Proportionalitätsfaktor ergibt sich aus der Auswertung der FE-Simulationen zu

$$\frac{t_\mathrm{s,FEM}}{t_\mathrm{p,FEM}} = 1{,}38 \pm 0{,}10\,. \tag{4}$$

Durch den Vergleich von Messung und Simulation ergibt sich schließlich die tatsächliche Eindringtiefe:

$$\frac{t_\mathrm{s}}{t_\mathrm{s,FEM}} = 1{,}02 \pm 0{,}29\,. \tag{5}$$

Vereinfachtes Prozessmodell zur Abschätzung der durch das Festwalzen eingebrachten Eigenspannungen

Zusammenfassend kann also der Verlauf der Eigenspannungen in Axialrichtung σ_e über dem Abstand von der Oberfläche x gemäß Abb. A.4 als linear angenommen werden mit

$$\sigma_{\mathrm{e}} = R_{\mathrm{p0,2}} \cdot \left(\frac{x}{t_{\mathrm{s}}} - 1 \right) \tag{6}$$

für $0 < x < t_{\mathrm{s}}$.

Die Eindringtiefe der Eigenspannungen t_{s} wird über die Proportionalität zur Tiefe der plastischen Zone t_{p} berechnet; t_{p} wird dabei über eine Kombination von Hertzschem und Prandtlschem Modell ermittelt. Mit den mittleren Werten aus Tab. A.1 errechnet sich die fiktive mittlere Flächenpressung für das Hertzsche Modell zu

$$p_{\mathrm{m,Hertz}} = \frac{2{,}13 \pm 0{,}37}{0{,}98 \pm 0{,}08} p_{\mathrm{m,Prandtl}} = \frac{2{,}13 \pm 0{,}37}{0{,}98 \pm 0{,}08} \cdot 2{,}97 \cdot \sigma_{\mathrm{F}} = (6{,}46 \pm 1{,}24) \cdot \sigma_{\mathrm{F}} \approx (6{,}46 \pm 1{,}24) \cdot R_{\mathrm{p0,2}}. \tag{7}$$

Damit ist aus den üblichen Beziehungen für den Hertzschen Kontakt die Kontakthalbbreite (die kleine Halbachse der Kontaktellipse) b_{Hertz} abzuschätzen. Aus b_{Hertz} wird über die Prandtlsche Lösung und die entsprechende Korrektur zur FEM-Lösung die Eindringtiefe der plastischen Zone abgeschätzt:

$$t_{\mathrm{p,FEM}} = \frac{1}{0{,}67 \pm 0{,}08} \cdot t_{\mathrm{p,Prandtl}} = \frac{1}{0{,}67 \pm 0{,}08} \cdot 1{,}414 \cdot b_{\mathrm{Prandtl}} = (2{,}11 \pm 0{,}25) \cdot b_{\mathrm{Prandtl}} \approx$$
$$\approx (3.05 \pm 0{,}61) \cdot b_{\mathrm{Hertz}} \tag{8}$$

Die tatsächliche Eindringtiefe der Eigenspannungen ergibt sich schließlich aus (3, 4, 5, 8) zu

$$t_{\mathrm{s}} = (1{,}02 \pm 0{,}29) \cdot t_{\mathrm{s,FEM}} = (1{,}02 \pm 0{,}29) \cdot (1{,}38 \pm 0{,}10) \cdot t_{\mathrm{p,FEM}} = (2{,}97 \pm 0{,}94) \cdot b_{\mathrm{Prandtl}} \approx$$
$$\approx (4{,}43 \pm 1{,}58) \cdot b_{\mathrm{Hertz}} \tag{9}$$

Beanspruchung und Stabilität der Eigenspannungen

Die Gesamtspannung im Bauteil – also die Summe aus Eigen- und Lastspannungen – darf an keiner Stelle und zu keiner Zeit die Fließspannung überschreiten; andernfalls kommt es zu plastischem Fließen und zu sofortigem Abbau der Spannungen bis auf die Fließspannung. Bei festgewalzten Bauteilen unter (umlaufender) Biegebeanspruchung ist direkt an der Bauteiloberfläche die Vergleichsspannung nach Tresca gleich der Summe aus Eigen- und Lastspannungen in Axialrichtung. Es liegt also nahe anzunehmen, dass die verbleibenden Eigenspannungen genau der Fließspannung abzüglich der höchsten im Betrieb auftretenden Lastamplitude entsprechen.

Diese Hypothese wird durch Versuchsergebnissen an festgewalzten Laborproben bestätigt; Abb. A.6 zeigt den Eigenspannungsverlauf nach dem Festwalzen, nach 10 und nach 1000 Lastwechseln unter Umlaufbiegebeanspruchung mit einer Lastamplitude von 500 MPa. Bereits nach nur 10 Zyklen haben sich die Eigenspannungen weitgehend abgebaut; nach 1000 Zyklen liegen sie bei etwa 50 bis 100 MPa. Bei kleinerer Lastamplitude von 360 MPa bauen sich die Eigenspannungen nicht so stark ab und sind mit dem Eigenspannungsverlauf nach 10 Zyklen und 500 MPa Lastamplitude vergleichbar. Diese Eigenspannungsverteilungen ergeben sich gemäß obiger Hypothese durch Subtraktion der Lastamplitude von der Fließspannung (im Gegensatz zur Fließgrenze ist hier besser der Mittelwert aus Fließgrenze und Zugfestigkeit zu verwenden, für 25CrMo4 ca. 600 MPa).

Umgelegt auf biegebeanspruchte Bauteile bedeutet dies, dass sich durch den Betrieb die Eigenspannung an der Oberfläche um den Betrag der höchsten auftretenden Lastamplitude verringern wird. Bei Höchstlasten in der Größenordnung von 150 MPa für 25CrMo4 verbleiben damit immer noch oberflächennahe Eigenspannungen von etwa 250 bis 350 MPa stabil über die Einsatzdauer.

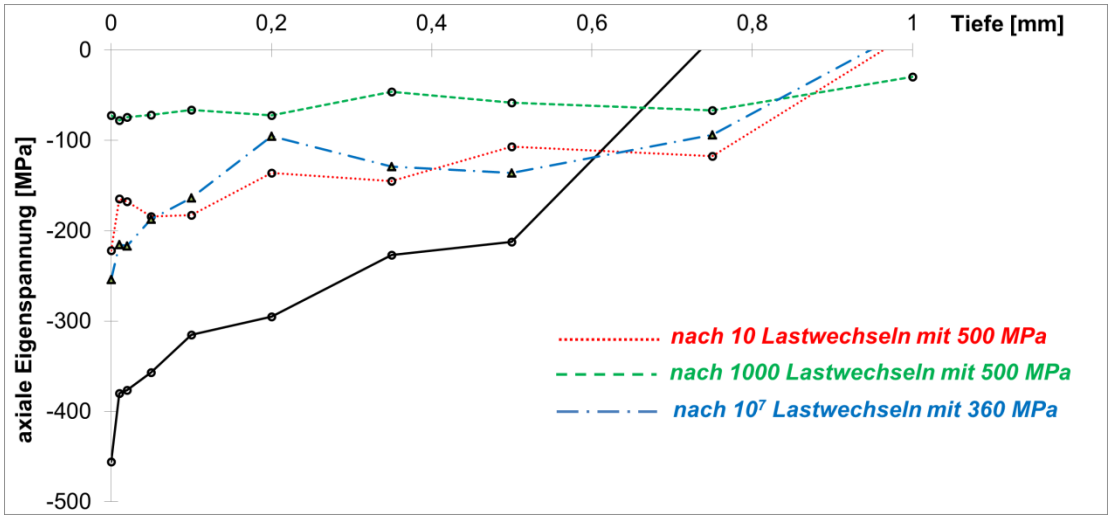

Abb. A.6: Abbau von Eigenspannungen – mittels Röntgendiffraktometrie ermittelte Eigenspannungsverläufe an festgewalzten Laborproben; nach dem Festwalzen, nach 10 und nach 1000 Lastwechseln mit einer Amplitude von 500 MPa bzw. nach 10^7 Lastwechseln mit einer Amplitude von 360 MPa (Umlaufbiegung).

Eigenspannungen und Schadenstoleranz

Da sich die Eigenspannungen den Lastspannungen als statische Mittelspannungen überlagern, kann der Sicherheitsnachweis einerseits mit herkömmlichen Methoden der Betriebsfestigkeit erfolgen. Andererseits kann auch ein Nachweis der Gebrauchseignung unter Annahme eines bestehenden Ermüdungsrisses geführt werden. Die Größe des anzunehmenden Risses richtet sich dabei nach der Detektionsgrenze des in der Instandhaltung angewandten zerstörungsfreien Prüfverfahrens, wodurch eine Abschätzung von Inspektionsintervallen mithilfe von Methoden der Schadenstoleranz möglich wird [6].

Zusammenfassung

Festwalzen stellt ein einfaches und kostengünstiges Verfahren zur Erhöhung der Schadenstoleranz von Bauteilen durch Einbringen von Druckeigenspannungen dar. Die in diesem Beitrag vorgestellten, durch Versuchsergebnisse abgesicherten Faustformeln erlauben einen Vergleich von Festwalzwerkzeugen hinsichtlich der erreichbaren Eindringtiefen der Druckeigenspannungen und der dazu notwendigen Festwalzkräfte sowie eine Abschätzung des Eigenspannungsabbaus aufgrund betrieblicher Lasten. Damit kann bereits in den ersten Stadien der Auslegung eine Entscheidung getroffen werden, ob der Einsatz des Festwalzverfahrens nach technisch-wirtschaftlichen Gesichtspunkten notwendig und sinnvoll erscheint.

Danksagung

Der österreichischen Bundesregierung (insbesondere dem Bundesministerium für Verkehr, Innovation und Technologie und dem Bundesministerium für Wirtschaft, Familie und Jugend), vertreten durch die Österreichische Forschungsförderungsgesellschaft mbH (FFG), und den Ländern Steiermark und Tirol, vertreten durch die Steirische Wirtschaftsförderungsgesellschaft mbH (SFG) sowie die Standortagentur Tirol, wird für die Förderung im Rahmen des COMET Förderprogramms herzlich gedankt.

References for Publication A

[1] Zerbst, U., et al.: Safe life and damage tolerance aspects of railway axles – A review. Engng Fract Mech 98 (2013) 214-271

[2] MARAXIL: Manufacturing railway axles with improved lifetime. http://maraxil.mecc.polimi.it/WP2.html (zuletzt abgerufen am 27.03.2014)

[3] Shaw, M. C., DeSalvo, J. The Role of Elasticity in Hardness Testing. Metals Engineering Quarterly 12(2), 1-7, (1972)

[4] Hill, R.: The mathematical theory of plasticity. Oxford University Press, Ely House, London W. (1971)

[5] Rees, D.W.A.: Basic Engineering Plasticity: An introduction with engineering and manufacturing applications. Elsevier Ltd. (2006).

[6] Lütkepohl, K., Esderts, A., Luke, M., Varfolomeev, I.: Sicherer und wirtschaftlicher Betrieb von Eisenbahnfahrwerken. Band 1-3 (2009)

Publication B: Modified NASGRO equation for physically short cracks

Modified NASGRO equation for physically short cracks

J. Maierhofer[1,2], R. Pippan[2], H.-P. Gänser[1]

[1]Materials Center Leoben Forschung GmbH, Roseggerstraße 12, A-8700 Leoben;
juergen.maierhofer@mcl.at; hans-peter.gaenser@mcl.at
[2]Erich Schmid Institute of Materials Science, Jahnstraße 12,A-8700 Leoben;
reinhard.pippan@oeaw.ac.at

Abstract

A typical fatigue crack growth curve consists of the threshold region, the Paris region (linear in a logarithmically scaled diagram) and the transition region from the Paris region to unstable crack growth. For cracks exceeding a certain material-dependent length, this curve depends only on the load ratio R and is well described by commonly accepted crack growth models such as the Forman/Mettu (NASGRO) equation. However, cracks below this length typically grow significantly faster due to the absence of crack-closure effects, leading to an additional dependence of the crack growth curve on the crack extension Δa. In this paper, a simple analytical model for describing the crack growth behavior for any crack length and load ratio R is presented. For the QT steel 25CrMo4, the model is applied to describe the crack growth behavior for different crack length and load ratios between -3 and 0.5.

Introduction

To estimate life-time or inspection intervals of components it is crucial to obtain a reliable estimate for the growth of fatigue cracks which may potentially pre-exist or have been initiated during operation. The analytical description of crack growth under cyclic loading, with the maximum stress σ_{max}, the minimum stress σ_{min} and the stress range $\Delta\sigma = \sigma_{max} - \sigma_{min}$ as well as the respective stress intensity factors K_{max}, K_{min}, ΔK for any load ratio $R = \sigma_{min} / \sigma_{max} = K_{min} / K_{max}$ and crack extension Δa, is based on the crack growth equations according to Erdogan/Ratwani [1] and Forman/Mettu [2] including Newman's model for plasticity-induced crack closure [3]. A summary and short discussion of these equations can be found in [4]. It is known that short cracks are able to grow below the threshold for long crack growth, and that they can grow significantly faster than long cracks at the same cyclic stress intensity factor range [5, 6, 7]. Commonly used crack growth models cannot describe short crack growth with sufficient accuracy or do not consider this behavior at all, which may lead to non-conservative lifetime predictions (cf. Fig. B.1) with potentially disastrous consequences.

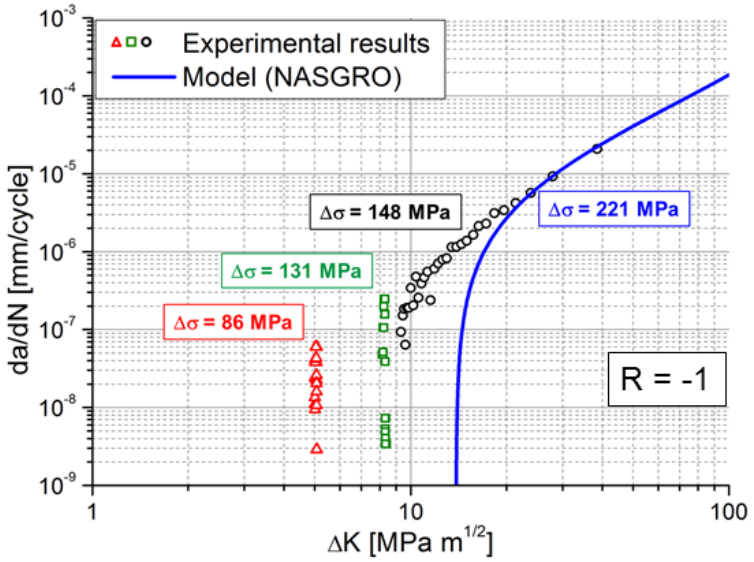

Fig. B.1: Crack propagation behavior in a bending sample with a 1 mm deep notch. The data illustrates that conventional models are not able to describe the behavior of short cracks. The final crack extension Δa at the stress range of 131 MPa is about 185 µm. In deep sharp notched specimens, the typical crack extension for crack arrest is between 1 mm and 3 mm at a load ratio of $R = -1$.

Nomenclature

α	constraint factor, $\alpha = 1$ for plane stress and $\alpha = 3$ for plane strain	$\Delta K_{th,lc}$	long crack growth threshold stress intensity factor range
Δa	crack extension length	K	stress intensity factor
a_0	notch depth	K_c	fracture toughness
$a_{0,H}$	fictitious intrinsic length scale following El Haddad	K_{max}	maximum stress intensity factor
a	total crack length	K_{min}	minimum stress intensity factor
A_0, A_1,A_2, A_3	polynomial coefficients of Newman's crack opening function	K_{op}	opening stress intensity factor
B	thickness of specimen	l_i	fictitious length scales
C	crack growth constant	L	length of specimen
C_{th}	curve control coefficient	m	Paris exponent
da/dN	fatigue crack growth rate	p,q	empirical constants describing the curvatures that occur near the threshold and near the instability region of the crack growth curve, respectively
f	crack opening function	R	load ratio
F	crack velocity factor	S	span
F_{lc}	crack velocity factor according to long cracks	$\Delta\sigma$	stress range
F_a	applied load amplitude	σ_F	flow stress (average between uniaxial yield stress and uniaxial tensile strength)
J_i	initiation fracture toughness	σ_{max}	maximum applied stress
ΔK	stress intensity factor range	σ_{min}	minimum applied stress
ΔK_0	stress intensity factor range for long crack growth at R = 0	v_i	weighting factors
ΔK_{th}	threshold of stress intensity factor range for crack propagation	W	width of specimen
$\Delta K_{th,eff}$	intrinsic (effective) threshold stress intensity factor range		

There are different types of short cracks which are broadly classified in microstructurally short cracks, mechanically short cracks, physically short cracks and chemically short cracks [5]. Microstructurally short cracks are comparable in size to the scale of the characteristic microstructural dimension. Mechanically short cracks are comparable to the near-tip plastic zone, or are engulfed by the plastic strain field of a notch. Physically short cracks are significantly larger than the characteristic microstructural dimension and the scale of local plasticity, and typically have lengths smaller than a millimeter or two. Chemically short cracks exhibit apparent anomalies in their propagation rate below a certain crack size [5]. The purpose of the present contribution is to create a crack growth model which is able to describe the growth rate of cracks of arbitrary length under the condition of small scale yielding, i.e., for physically short cracks. At first, the approach describing the crack growth behavior by considering the build-up of crack closure will be described (Section 2), followed by experimental verification of the modified NASGRO equation (Section 3).

Analytical description of the crack growth behavior

The following considerations on crack growth behavior are based on a mechanical model as shown in Figure B.2a. Starting from a sharp notch with depth a_0, a crack of length Δa is growing. The sharp notch can be regarded as a crack of length a_0 which is not subject to any crack closure. Therefore the stress intensity factor range is calculated via $\Delta K \sim \Delta\sigma(\pi a)^{1/2}$ using the total crack length $a = a_0 + \Delta a$, whereas the build-up of crack closure does only occur on the crack extension Δa.

In what follows, the NASGRO equation according to Forman/Mettu [2],

$$\frac{\mathrm{d}a}{\mathrm{d}N} = C \cdot F \cdot \Delta K^{m} \cdot \frac{\left(1-\frac{\Delta K_{\mathrm{th}}}{\Delta K}\right)^{p}}{\left(1-\frac{K_{\max}}{K_{\mathrm{c}}}\right)^{q}} = C \cdot F \cdot \Delta K^{m-p} K_c^{\,q} \frac{(\Delta K - \Delta K_{\mathrm{th}})^{p}}{(K_{\mathrm{c}} - K_{\max})^{q}}, \tag{1}$$

will be discussed and then modified to take account of the short crack behavior (i.e., the deviation from the long crack propagation behavior for small Δa).

Eq. (1) represents all three branches of the crack growth curve (Fig. B.2b): the fatigue crack

growth threshold ΔK_{th} gives the position of branch I; the parameters C and m and the crack velocity factor F discussed below describe the Paris region (branch II); the fracture toughness K_c determines the transition to unstable crack growth (branch III). In addition, the curvatures of the transitions between the different branches can be adjusted by means of the parameters p and q.

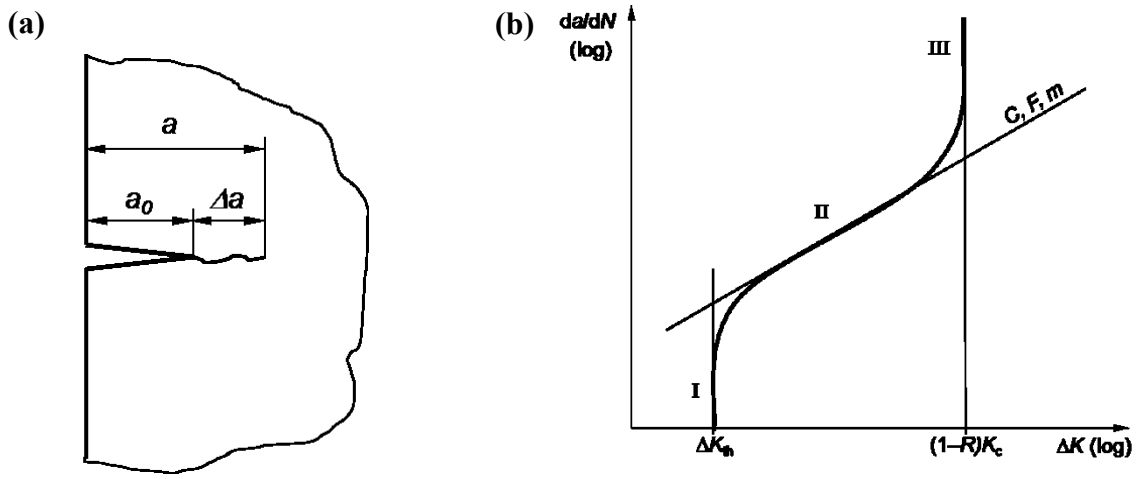

Fig. B.2: (a) Schematic illustration of the used mechanical model; (b) typical shape of fatigue crack growth curve for long cracks for a constant load ratio R.

However, the exact position of each of the three branches is influenced by the load ratio R: although not denoted explicitly in Eq. (2), the threshold ΔK_{th} (describing branch I) and the crack velocity factor F (describing the location of branch II) depend on R. Likewise, the location of branch III in the da/dN vs. ΔK curve also depends on R, because $K_{max} = \Delta K / (1-R)$. Therefore, for $K_{max} = K_c$ one obtains $\Delta K = (1\text{-}R)\, K_c$. All influences from load ratio and crack opening behavior will be discussed in more detail below.

Setting $p = m$ and $q = 1$ independent of R for simplicity, one obtains

$$\frac{\mathrm{d}a}{\mathrm{d}N} = C \cdot F \cdot \frac{\left(\Delta K - \Delta K_{th}\right)^m}{1 - \dfrac{K_{max}}{K_c}} = C \cdot F \cdot \frac{\left(\Delta K - \Delta K_{th}\right)^m}{1 - \dfrac{1}{1-R}\dfrac{\Delta K}{K_c}}. \qquad (2)$$

To adjust the simplified NASGRO equation (2) to the behavior of short cracks, one has to take into account

- that short cracks are able to grow below the threshold for long crack growth and

- that short cracks grow significantly faster than long cracks at the same stress intensity factor range, most notably in the low and medium near threshold regime, the Paris region.

The former effect can be modeled by introducing a dependence on the crack extension Δa into the expression for the crack growth threshold ΔK_{th}, the latter effect by modifying the crack velocity factor F according to the influence of Δa.

Analytical description in the threshold region

In the original formulation of the NASGRO equation [2, 4], the dependence of the threshold for crack growth propagation on the load ratio R is approximated by

$$\Delta K_{th} = \Delta K_0 \sqrt{\frac{a}{a + a_{0,H}}} \left[\frac{1 - f}{(1 - A_0)(1 - R)} \right]^{-(1 + C_{th} R)}, \tag{3}$$

where ΔK_0 is the threshold for long crack growth at $R = 0$, and C_{th} and A_0 are additional adjustment parameters.

The crack opening function $f = K_{op} / K_{max}$, i.e., the ratio of crack opening stress versus maximum applied stress, is used to model the influence of various crack closure mechanisms. Newman [3] achieved, based on finite element simulations of plasticity-induced crack closure for long cracks, the following analytical approximation for the crack opening function:

$$f = \begin{cases} \max(R; A_0 + A_1 R + A_2 R^2 + A_3 R^3) & \text{for } R \geq 0, \\ A_0 + A_1 R & \text{for } -2 \leq R < 0, \\ A_0 - 2A_1 & \text{for } R < -2 \end{cases} \tag{4}$$

with

$$\begin{aligned} A_0 &= \left(0{,}825 - 0{,}34\alpha + 0{,}05\alpha^2\right) \left[\cos\left(\frac{\pi \sigma_{max}}{2\sigma_F} \right) \right]^{1/\alpha}, \\ A_1 &= \left(0{,}415 - 0{,}071\alpha\right) \frac{\sigma_{max}}{\sigma_F}, \\ A_2 &= 1 - A_0 - A_1 - A_3, \\ A_3 &= 2A_0 + A_1 - 1. \end{aligned} \tag{5}$$

In what follows, the values $\sigma_{max} / \sigma_F = 0.3$ and $\alpha = 3$ are assigned, as it applies for approximate plane strain condition and largely elastic crack behavior; for a more detailed discussion of these parameters see [3, 4].

In Eq. (3), $a_{0,H}$ is a fictitious intrinsic length scale based on the concept of El Haddad [8] for the approximate consideration of short crack effects. As a consequence of this approximation a crack of total length $a = 0$ shows a threshold value of 0. Such an increase of ΔK_{th} with crack extension might be interpreted by the build-up of crack closure until $a = a_{0,H}$. At least in the presence of an initial notch a_0, see Fig. B.2a, this concept proves to be unsustainable because only the crack extension Δa and not the total crack length a is relevant to the build-up of crack closure effects. Furthermore, also in the absence of crack closure the threshold value is not 0 but equal to the effective threshold for crack propagation $\Delta K_{th,eff}$. For these reasons, the application of the El Haddad correction is not considered (i.e., $a_{0,H} = 0$), and one obtains

$$\Delta K_{th,lc} = \Delta K_0 \left[\frac{1-f}{(1-A_0)(1-R)} \right]^{-(1+C_{th}R)} \tag{6}$$

In what follows, Eq. (6) is exclusively used to describe the R dependence of the long crack threshold.

For the description of the threshold build-up starting from the intrinsic value of $\Delta K_{th,eff}$ at a crack extension of $\Delta a = 0$ to the long crack growth threshold $\Delta K_{th,lc}$ at large Δa, the empirical approach

$$\Delta K_{th} = \Delta K_{th,eff} + (\Delta K_{th,lc} - \Delta K_{th,eff}) \cdot \left[1 - \sum_{i=1}^{n} v_i \cdot \exp\left(-\frac{\Delta a}{l_i} \right) \right] \tag{7}$$

with the constraint

$$\sum_{i=1}^{n} v_i = 1 \tag{8}$$

is proposed. The l_i can be interpreted as fictitious length scales for the formation of crack closure effects (see Fig. B.3), similar to $a_{0,H}$, and may be determined in conjunction with the v_i

by fitting of the experimentally obtained crack growth resistance curve (ΔK_{th} plotted against Δa), as shown later. The basic physical idea behind this approach is that each closure mechanism requires a certain crack extension length to build up completely. A similar approach has been proposed by McEvily [9], using a single fictitious length related to the crack opening stress intensity factor.

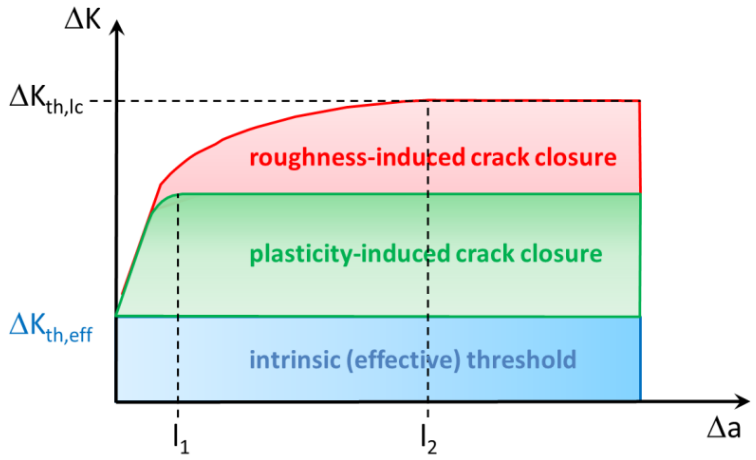

Fig. B.3: Illustration of the build-up of crack closure due to plasticity induced crack closure and roughness induced crack closure mechanisms with fictitious length scales l_i.

Analytical description in the Paris region

In the original formulation of the NASGRO equation [2, 4], the crack velocity factor

$$F = \left(\frac{1-f}{1-R} \right)^{m} \tag{9}$$

describes the position of region II depending on the load ratio R for long cracks (large crack extensions Δa).

For cracks with arbitrary crack extension Δa, an empirical approach for the crack velocity factor F is developed similar to the adjustment in the threshold region. Because the crack growth rate is influenced by the same crack closure mechanisms as the crack growth threshold, in analogy to Eq. (7) the approximation

$$F = 1 - (1 - F_{\mathrm{lc}}) \cdot \left[1 - \sum_{i=1}^{n} v_i \cdot \exp\left(- \frac{\Delta a}{l_i} \right) \right] \tag{10}$$

with

$$F_{\mathrm{lc}} = \left(\frac{1 - f}{1 - R} \right)^{m} \tag{11}$$

and unchanged values for the l_i and v_i is chosen in place of Eq. (9).

Finally it should be noted that in reality the relative contributions of crack closure – i.e. the values of v_1 and v_2 – depend on ΔK and R. In addition the characteristic lengths to build up the different crack closure mechanisms are functions of ΔK and R. Therefore the v_i and l_i are affected by ΔK and R. The assumption that the v_i and l_i are independent of ΔK should be well fulfilled near the threshold and lower Paris regime. In this case the different contributions of crack closure are similar to those at the threshold. However in the mid and upper Paris regime this is different. The plasticity induced crack closure becomes more dominant compared to roughness and oxide induced crack closure, i.e., the relative contributions of plasticity induced crack closure v_1 increases and the relative contribution of roughness and oxide induced crack closure v_2 and v_3 decrease. Furthermore, the characteristic length l_1 to build up plasticity induced crack closure increases, because the plastic zone size increases. If $l_1 << l_2$ and $v_1 \approx v_2$ (see next section), the increase of l_1 is partly compensated by the change of the ratio v_1/v_2. Hence the simplification that F does not depend on ΔK should give a satisfactory approximation of the real increase of crack closure in the near threshold as well as in the Paris region.

Figure B.4b shows the dependence of the crack velocity factor F on the load ratio R and the crack extension Δa in graphical form. At all load ratios R below 0.5, a clear difference between short and long crack behavior is recognized.

The crack velocity factor F is based on Newman's crack opening function f, Figure B.4a, and adjusted according to the crack extension, cf. Eqns (10) and (11). Basically, $F = 1$ is assigned to the unreduced growth rate of a crack where no crack shielding occurs, i.e., where the maximum stress intensity factor in a load cycle K_{max} acts to its full extent as a driving force for crack opening K_{op}, or where $f = K_{\mathrm{op}} / K_{\mathrm{max}} = 1$. Wherever crack closure mechanisms are present, one obtains $f < 1$ and $F < 1$.

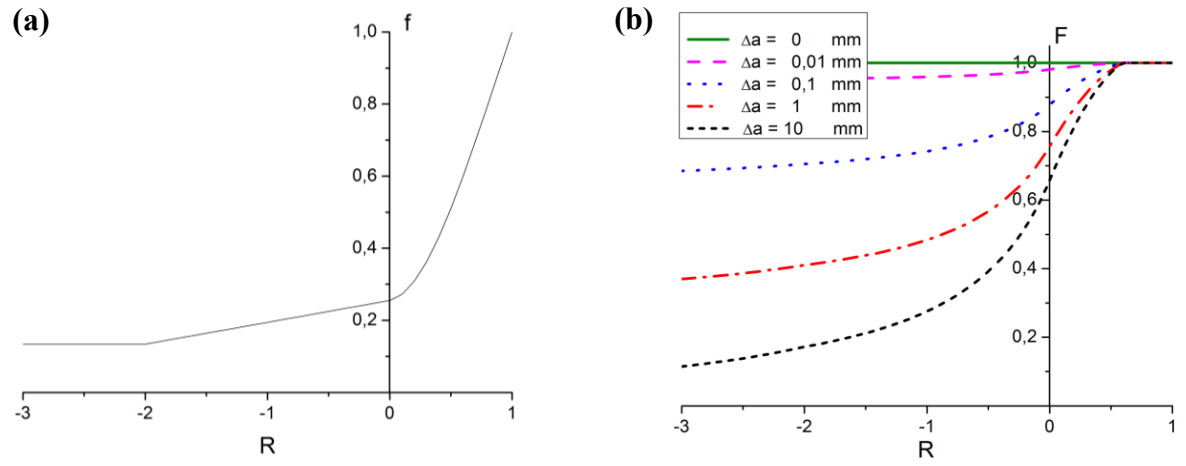

Fig. B.4: (a) Crack opening function f from Eq. (4) and (b) crack velocity factor F from Eq. (10) for different crack extensions Δa depending on the load ratio R.

Experimental verification

For model calibration, experiments on typical standard fracture mechanic samples – i.e. deep notched specimens – were tested. For the verification of the proposed equation to describe the fatigue crack propagation, in addition different fatigue experiments on short notches were performed.

Material and experimental procedure

As material for the experimental investigations, the QT steel 25CrMo4 widely used for drivetrain components was chosen. The material has a bainitic microstructure and a hardness of ~245 HV10. In the tensile test, a 0.2% offset yield stress of 512 MPa, a tensile strength of 674 MPa, and an elongation at fracture of 18.9% are obtained.

For determining the fatigue crack propagation behavior, SENB (Single Edge Notched Bending) specimens measuring L = 100 mm, B = 6 mm, W = 20 mm (cf. Fig. B.5a)with different notch depths a_0 (0.35mm, 1 mm, 5.3 mm) were machined. The latter one corresponds to a sample for a standard fatigue crack growth experiment. The notches were sharpened by means of razor blade polishing with diamond paste (1 µm). The samples were then compression pre-cracked at a load ratio of $R = 10$ to obtain a fatigue pre-crack (cf.

Fig. B.5b). Due to tensile residual stresses from compression pre-cracking, the pre-crack is fully open so that crack closure effects can be excluded at the beginning of the crack growth experiment, see also [10, 11]. The applied stress intensity to generate the pre-crack was taken as small as possible – ΔK of about 20 MPa $m^{1/2}$ – in order to reduce the residual stress affected region in front of the pre-crack , and more than 10^4 cycles were used. The pre-crack measured from the notch root has typically a length between 20 – 80 µm. The notch root radius was usually smaller than 10 µm hence standard fracture mechanics equations to determine ΔK could be applied.

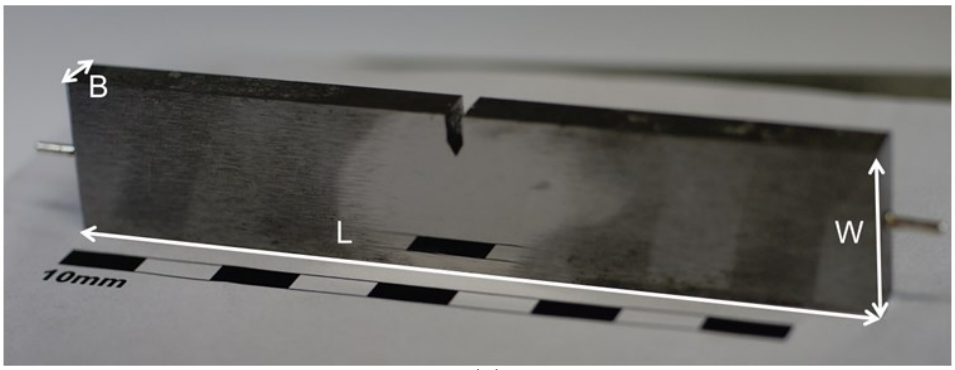

(a)

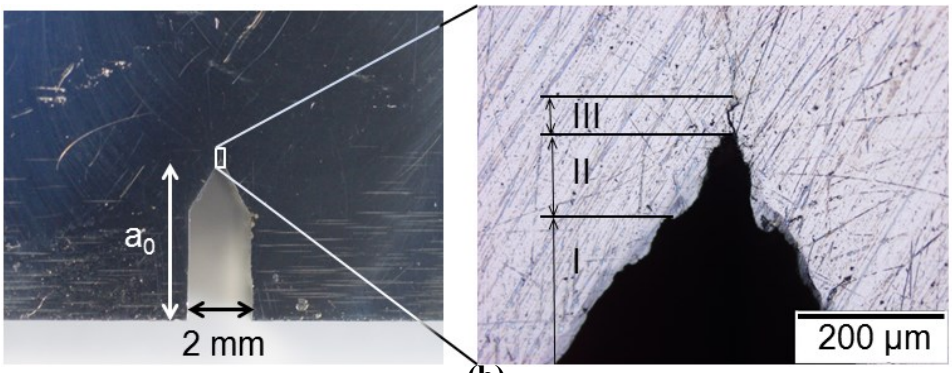

(b)

Fig. B.5: (a) SENB specimen with thickness B = 6 mm, length L = 100 mm and width W = 20 mm. (b) notch details: I machined notch, II razor blade polishing, III compression pre-crack.

The experiments are performed at room temperature under laboratory conditions for three different load ratios R of 0.5, –1 and –3. The samples are subjected to cyclic loading under eight-point bending (cf. Fig. B.6) in a resonance test rig at a testing frequency of 108 Hz. The crack growth is measured using the direct current potential drop (DCPD) method. Any temperature influence on the measured electric potential drop due to the Seebeck effect at

bimaterial junctions is excluded by periodic switching of the direction of the electric current and subsequent averaging. Crack arrest was defined as the (averaged) crack growth rate falling below a value of at most $6 \cdot 10^{-8}$ mm/cycle.

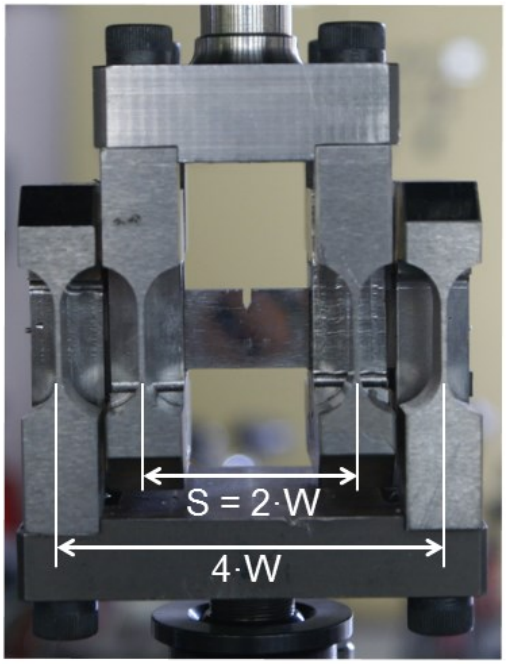

Fig. B.6: Loading setup for eight-point bending test.

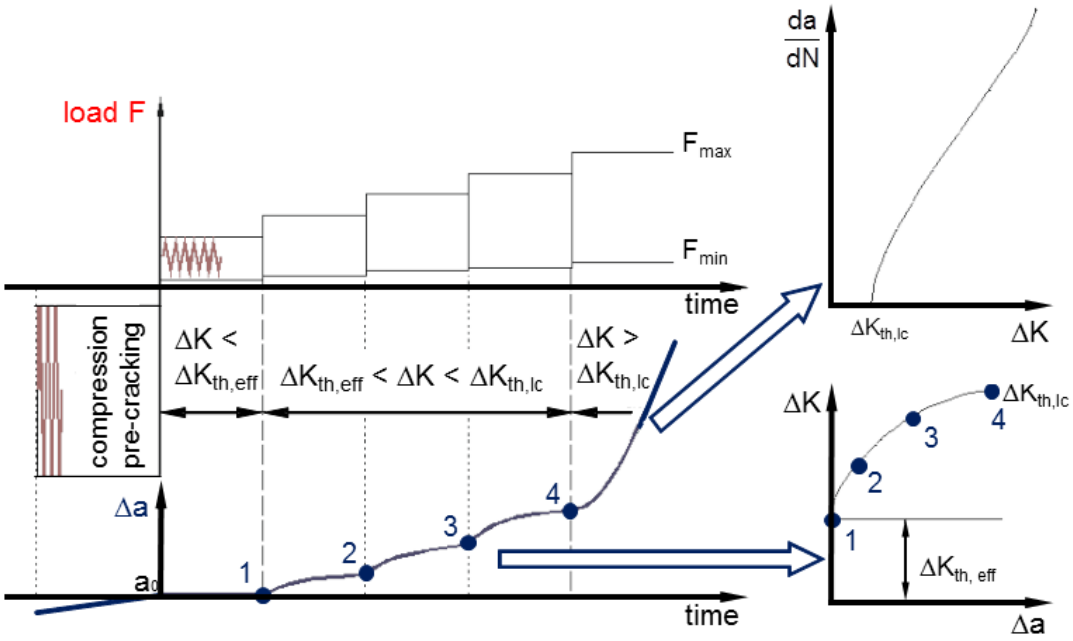

Fig. B.7: Schematic illustration of the loading procedure of a test to determine the R-curve for the fatigue crack propagation threshold and the fatigue crack growth curve at a constant load ratio [12].

The experiments are conducted under step-wise increasing constant loads as proposed by Tabernig [12]. The procedure is schematically illustrated in Fig. B.7. For load amplitudes which correspond to ΔK values smaller than the effective threshold $\Delta K_{th,eff}$, no crack propagation is observed. For load amplitudes which correspond to ΔK values larger than $\Delta K_{th,eff}$, the crack starts to propagate. The crack grows initially, but after a certain crack extension Δa crack arrest occurs due to the build-up of crack closure. Subsequently, the load is increased so that the crack can grow further. In this way, the resistance curve for the threshold of stress intensity factor range is obtained point by point (Fig. B.7, Fig. B.8). As soon as the crack starts to grow through, one gets the crack growth curve. At that crack extension, crack closure has already built up completely.

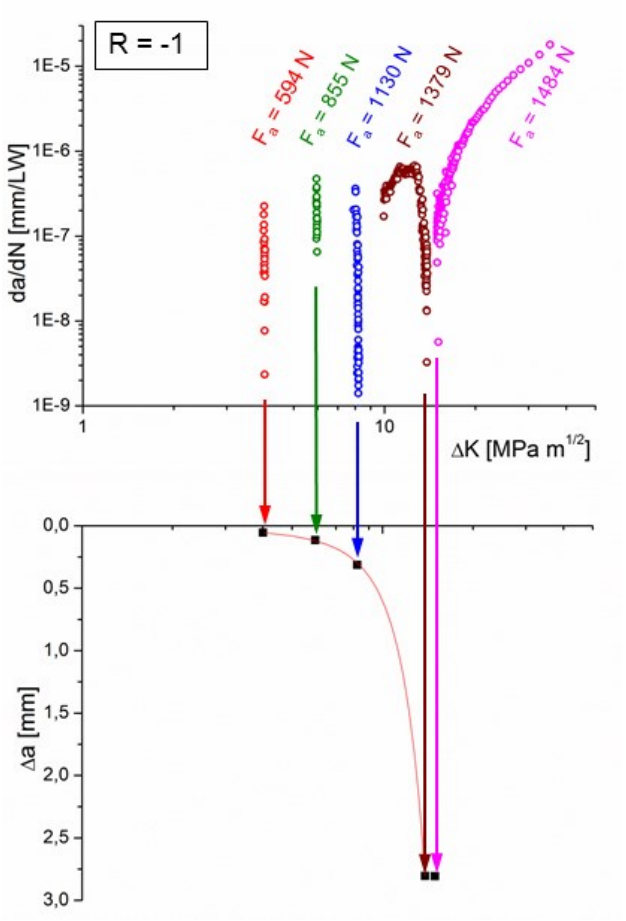

Fig. B.8: Experimental results for a constant load test at R = -1 with an initial notch depth of 5.12 mm; crack growth rate and derived points of the cyclic crack resistance curve.

The crack growth rates during these tests depend on the increased stress intensity range due to crack extension on the one hand, and on the increased crack growth threshold due to the

build-up of crack closure effects on the other hand. At very small crack extensions, the change in stress intensity range is negligible and crack closure effects build up rapidly, which leads to an immediate decrease of the crack growth rate and to crack arrest. For larger crack extensions, the build-up of crack closure becomes much slower (the resistance curve becomes very flat); under these conditions, the increase in stress intensity range due to crack extension may initially be more pronounced than the increase of the threshold value, which leads to an initial increase in crack growth rate until sufficient crack closure has developed, as in the case F_a = 1379 N in Fig. B.8.

Experimental results

Since all experiments started with closure free pre-cracks the results show the expected behavior as illustrated in Fig. B.7. For short crack extension the crack grows initially at stress intensity factor ranges below the threshold for the stress intensity factor range for long cracks. Due to the build-up of crack closure crack arrest occurs eventually. Fig. B.8 shows exemplarily the results for a specimen with an initial notch depth of 5.12 mm tested at a load ratio of R = -1. In this experiment, crack arrest occurs at four load amplitudes. The crack extensions Δa where the crack stops to propagate and the corresponding ΔK provide in this case four points of the resistance curve for the threshold of stress intensity factor range. The asymptotic value (for large Δa) of the resistance curve for ΔK_{th} is obtained from the threshold branch of the fatigue crack growth curve. The effective threshold – the starting point of the resistance curve for ΔK_{th} (Δa = 0) – has not been determined at all load ratios and crack lengths, as it is known to be typically about 2.5 MPa $m^{1/2}$ for ferritic steels.

Parameter determination

At first, the parameters for the load ratio dependent threshold of long cracks $\Delta K_{th,lc}$ in Eq. (6) are determined. To this purpose, the long crack thresholds $\Delta K_{th,lc}$ (R) are first extracted from the resistance curves recorded at different load ratios R (Fig. B.9) and then plotted against the load ratio R (Fig. B.10). Least-squares fitting of Eq. (6) to the data points in Fig. B.10 allows to determine the adjustment parameter C_{th}.

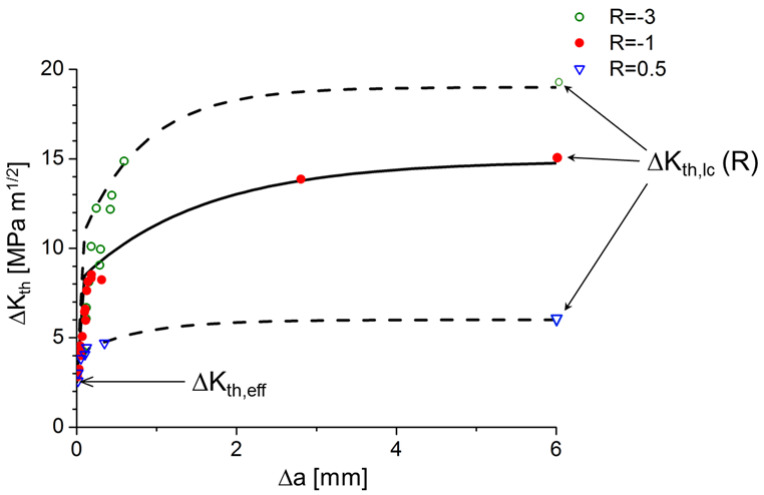

Fig. B.9: Crack resistance curves: crack growth threshold ΔK_{th} vs. crack extension Δa for different load ratios R – experimental data points and analytically predicted curves from Eq. (7).

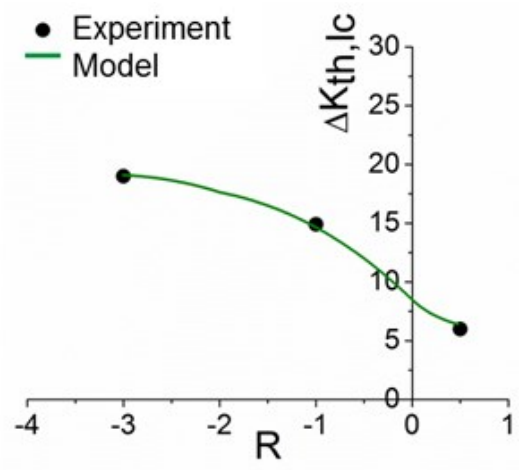

Fig. B.10: Load ratio dependent long crack growth threshold – experimental data points and analytically predicted curve from Eq. (6).

As it is assumed that the build-up of crack closure is similar at different load ratios, the fictitious length scales describing the build-up of crack closure can be estimated for a single resistance curve; in the present case, the resistance curve at $R = -1$ is chosen. $\Delta K_{th,eff}$ and $\Delta K_{th,lc}$ can be read directly from the resistance curve, cf. Fig. B.9. The length scales l_1 and l_2 together with the weighting factors v_1, v_2 are obtained by least-squares fitting of Eq. (7).

Now, the only remaining parameters are the crack growth constant C, the Paris exponent m, and the fracture toughness K_c. K_c is calculated using J_i from an experimentally determined

static crack resistance curve [4]; C and m are obtained by least-squares fitting of Eq. (2)[1]. The crack velocity factor F is calculated according to Eq. (10) with F_{lc} from Eq. (11), and ΔK_{th} is calculated according to Eq. (7) with $\Delta K_{th,lc}$ from Eq. (6). Newman's crack opening function f, Eq. (4), is used without any modification. The model parameters determined from the experiment are summarized in Table B.1.

Parameter	Value	Unit
C	760	nm / (MPa m1/2)
K_c	131,56	MPa m1/2
m	1,42	-
α	3	-
σ_{max}/σ_F	0,3	-
$\Delta K_{th,eff}$	2,5	MPa m1/2
ΔK_0	8,5	MPa m1/2
C_{th}	0,115	-
l_1	0,08	mm
l_2	1,55	mm
v_1	0,45	-
v_2	0,55	-

Table B.1: Parameters of the fatigue crack growth model for 25CrMo4.

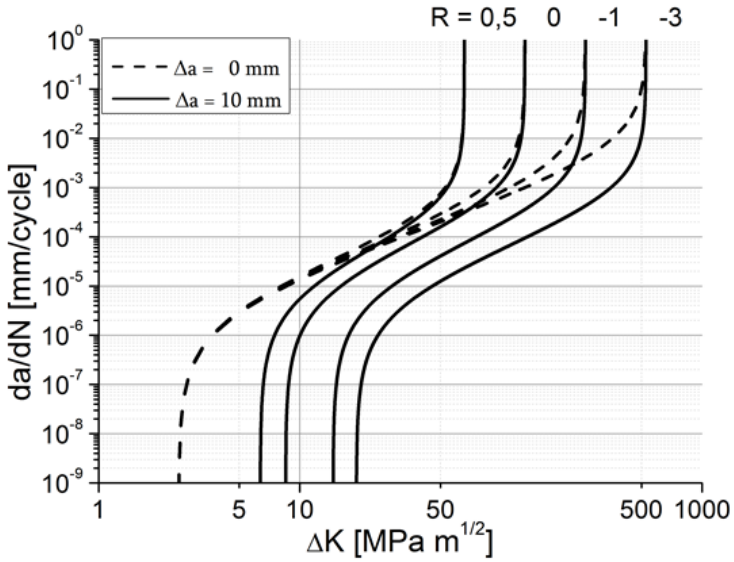

Fig. B.11: Calculated fatigue crack growth curves at a crack extension Δa of 0 and 10 mm and different load ratios R – analytical model.

[1] The relatively low value of 1.42 for m stems from the influence of the crack growth regions I and III. If only the data points from region II are used to fit the Paris equation $da/dN = C*\Delta K^n$, values between 2.7 and 2.8 are obtained for the Paris exponent n at all load ratios R.

Comparison of experimental results and model predictions

In Fig. B.11 the predictions of the proposed analytical crack growth model are shown for a crack starting from a very sharp notch ($\Delta a = 0$ mm) and for a crack after substantial growth ($\Delta a = 10$ mm), which can be seen as the limiting cases of a very short crack (no closure effects) and a crack where closure effects are fully present. This implies for constant amplitude loading and small scale yielding condition that no crack can grow faster than a very short crack (dashed line), and that no crack can grow slower than a long crack (full line) at a given load ratio R. It should be noted that the crack growth rate of a very short crack is in the threshold region (branch I) and in the Paris region (branch II) independent from the load ratio R; this can also easily be seen if the crack velocity factor F is evaluated for $\Delta a = 0$ (cf. Eq. (10) and Fig. B.4b).

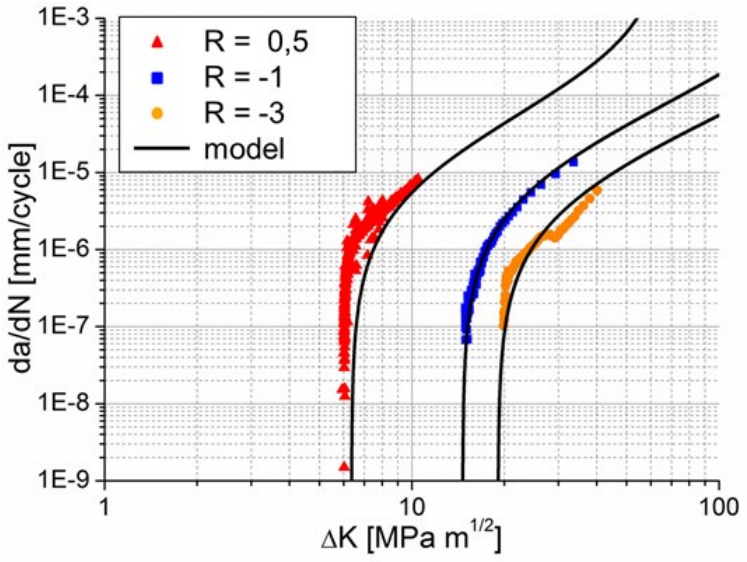

Fig. B.12: Comparison of experimentally determined long crack growth curves with curves calculated using the analytical model.

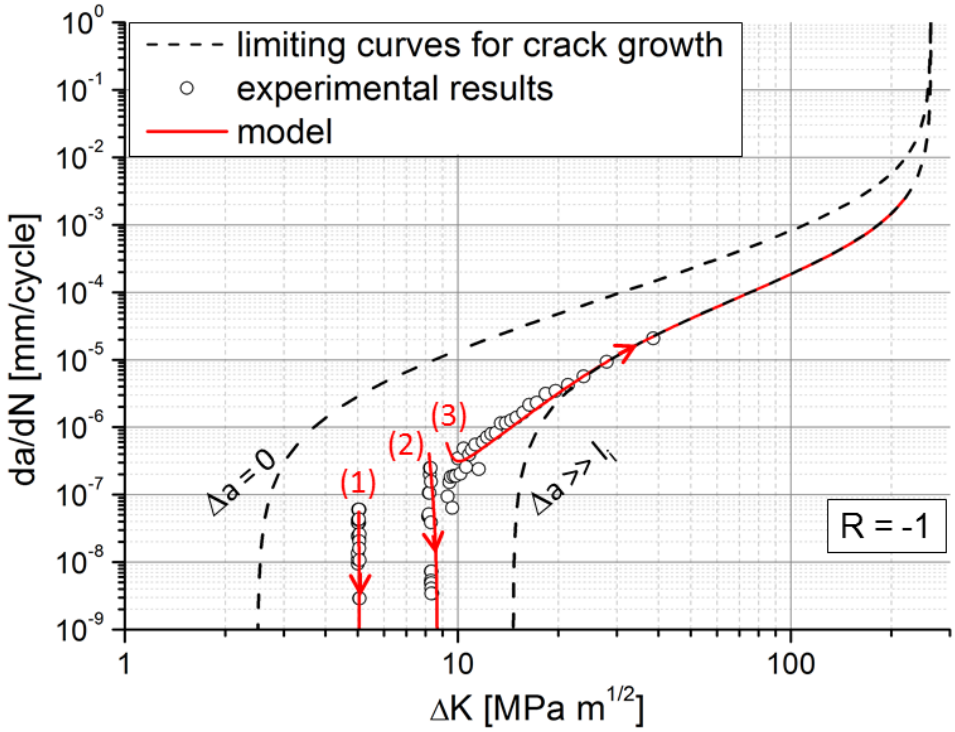

Fig. B.13: Growth of a short crack near the threshold region – comparison of experiment and prediction; initial crack length $a_0 = 0.81$ mm; start parameters for the three curves: curve (1): $\Delta K = 5.04$ MPa $m^{0.5}$, $a = 0.853$ mm; curve (2): $\Delta K = 8.19$ MPa $m^{0.5}$, $a = 0.94$ mm; curve (3): $\Delta K = 9.27$ MPa $m^{0.5}$, $a = 1$ mm.

The proposed equation permits to describe quite well the R dependence of long cracks and the fatigue crack growth behavior in deep sharp notches (the crack stopping behavior), as shown in Figs A.11 and A.12. However, more essential is the description of the propagation behavior from small flaws, as depicted in Fig. B.1. The growth of a short crack starting from a notch of depth $a_0 = 0.812$ mm ($R = -1$) is calculated and compared with the measured data. Good agreement between measurement and calculation is observed, cf. Figure B.13. The left limiting curve corresponds to a crack extension $\Delta a = 0$ (short crack behavior), the right to a very large Δa (long crack behavior). In the first two load steps the crack slows down and stops (curves 1, 2) due to the build-up of crack closure. Only after a further increase of the load amplitude the crack grows, after an initial slight deceleration, finally through, in the course of which it approaches the behavior of long cracks (curve 3).

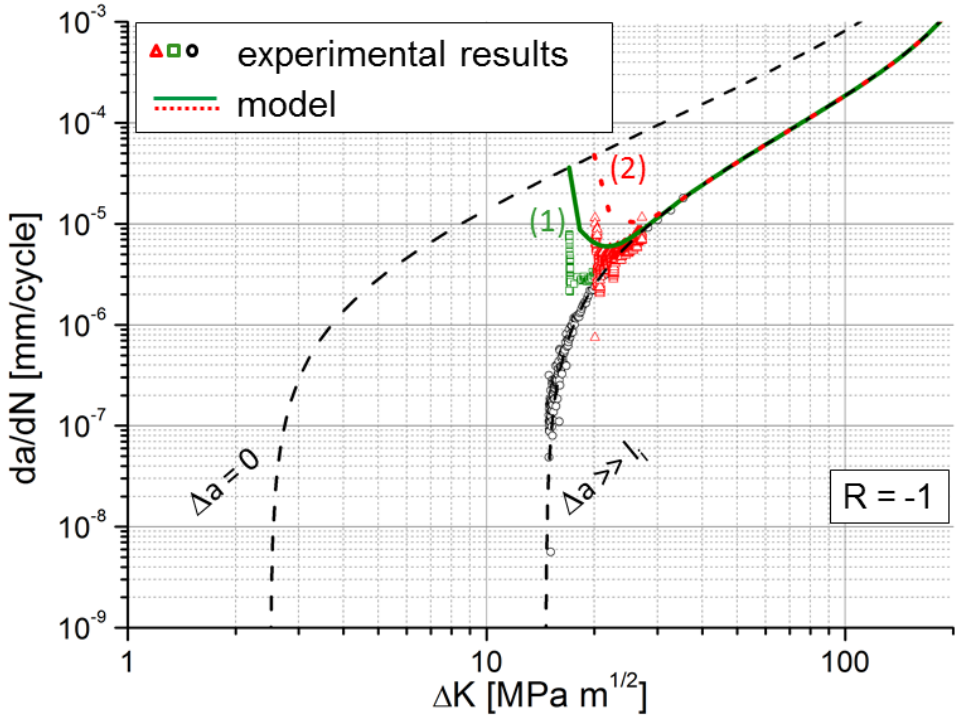

Fig. B.14: Growth of a short crack in the Paris region – comparison of experiment and prediction; curve (1): initial crack length $a_0 = 3.97$ mm, $\Delta K = 17$ MPa $m^{0.5}$, $a = 3.97$ mm; curve (2): initial crack length $a_0 = 3.975$ mm, $\Delta K = 20$ MPa $m^{0.5}$, $a = 3.975$ mm.

The growth of a crack starting from a sharp notch of depth $a_0 \sim 4$ mm ($R = -1$) in the Paris region is also calculated and compared with the measured data (Fig. B.14). The calculation inclines to about two times higher crack growth rates. It is supposed that this behavior is due to the much higher constant load in this test, leading to a larger plastic zone and increased plasticity-induced crack closure compared to the tests at stepwise increasing constant load used for model calibration.

Conclusions

It has been shown that, by mean of an analytical model for the build-up of crack closure effects with increasing crack extension Δa, a modified NASGRO crack growth equation can predict the crack growth rate for arbitrary crack lengths. With this model it is possible to predict fatigue lifetime or necessary inspection intervals more accurately in the context of

damage tolerant design and fitness-for-purpose assessments. It will be interesting to show whether the fictitious length scales, which have here been determined by curve fitting, can be related to flow stress and microstructural parameters; these investigations and experiments for load ratios $R < -1$ and $R > 0.5$ are currently performed. Still, even without this direct relation to physical length scales, the model has already proven useful for predicting the behavior of short cracks; in this sense, it will be interesting to explore potential conceptual links to the theory of critical distances as introduced by Taylor [13].

Acknowledgements

Financial support by the Austrian Federal Government (in particular from the Bundesministerium für Verkehr, Innovation und Technologie and the Bundesministerium für Wirtschaft, Familie und Jugend) and the Styrian Provincial Government, represented by Österreichische Forschungsförderungsgesellschaft mbH and by Steirische Wirtschaftsförderungsgesellschaft mbH, within the research activities of the K2 Competence Centre on "Integrated Research in Materials, Processing and Product Engineering", operated by the Materials Center Leoben Forschung GmbH in the framework of the Austrian COMET Competence Centre Programme, is gratefully acknowledged.

References for Publication B

[1] F. Erdogan, M. Ratwani. Fatigue and fracture of cylindrical shells containing a circumferential crack. Int J Fract Mech 6 (1970), 379-392.

[2] R.G. Forman, S.R. Mettu. Behavior of surface and corner cracks subjected to tensile and bending loads in Ti-6Al-4V alloy. In: Fracture Mechanics: 22nd Symposium, Vol. 1 (Eds H.A. Ernst, A. Saxena, D.L. McDowell), ASTM STP 1131, American Society for Testing and Materials, Philadelphia 1992, 519-546.

[3] J.C. Newman. A crack opening stress equation for fatigue crack growth. Int J Fract 24 (1984), R131-R135.

[4] Forschungskuratorium Maschinenbau. Fracture mechanics proof of strength for engineering components. 3rd ed. VDMA Verlag, Frankfurt 2009.

[5] S. Suresh, R.O. Ritchie. Propagation of short fatigue cracks. Int Metals Reviews (1984), Vol 29 No 6.

[6] R. Pippan, M. Berger, H.P. Stüwe. The influence of crack length on fatigue crack growth in deep sharp notches. Metall Trans 18A (1987), 429-435.

[7] J.C. Newman, E.P. Phillips, M.H. Swain. Fatigue-life prediction methodology using small-crack theory. Int J Fatigue (1999), Vol 21, Issue 2, 109-119.

[8] M.H. El Haddad, T.H. Topper, K.N. Smith. Prediction of non-propagating cracks. Eng Fract Mech 11 (1979), 573-584.

[9] A.J. McEvily, Z. Yang. The Growth of Short Fatigue Cracks under Compressive and/or Tensile Cyclic Loading. Metall Trans 22A (1991),1079-1082.

[10] R. Pippan, L. Plöchl, F. Klanner, H.P. Stüwe. The Use of Fatigue Specimens Precracked in Compression for Measuring Threshold Values and Crack Growth. J Test Eval 22 (1994), 98-103.

[11] B. Tabernig, R. Pippan. Determination of the length dependence of the threshold for fatigue crack propagation. Eng Fract Mech 69 (2002), 899-907.

[12] B. Tabernig, P. Powell, R. Pippan. Resistance Curves for the Threshold of Fatigue Crack Propagation in Particle Reinforced Aluminium Alloys, Fatigue Crack Growth Thresholds. Endurance Limits, and Designs, ASTM STP 1372, J.C. Newman, Jr and R. S. Piascik, Eds., American Society for Testing and Materials, West Conshohocken, PA, 2000.

[13] D. Taylor. The theory of critical distances. Eng Fract Mech 75 (2008), 1696-1705.

Publication C: Modified NASGRO equation for short cracks and application to the fitness-for-purpose assessment of surface treated components

Modified NASGRO equation for physically short cracks and application to the fitness-for-purpose assessment of surface-treated component

J. Maierhofer[1,2], R. Pippan[2], H.-P. Gänser[1]

[1]Materials Center Leoben Forschung GmbH, Roseggerstraße 12, A-8700 Leoben;
juergen.maierhofer@mcl.at; hans-peter.gaenser@mcl.at
[2]Erich Schmid Institute of Materials Science, Jahnstraße 12,A-8700 Leoben;
reinhard.pippan@oeaw.ac.at

Abstract

Fatigue cracks in cyclically loaded components usually initiate in areas of high stress concentration. Such stress concentrations do not only occur due to the geometrical design of a component, but also near material inhomogeneities or Foreign Object Damage (FOD). In the context of a fitness-for-purpose (FFP) assessment, it is important to estimate the fatigue crack growth rate as accurately as possible, e.g., for estimating inspection intervals for public transportation. However, the crack growth rate depends not only on the applied load and crack length, but also on residual stress fields introduced intentionally (surface treatment) or unintentionally (FOD or inappropriate handling).

In this work, an analytical model for describing the fatigue crack growth rate of short cracks (provided the conditions of LEFM are fulfilled) as well as of long cracks is developed. Also

the influence of residual stresses on the crack growth behavior is investigated. This permits to assess the combined influence of load stresses and residual stresses together with the build-up of crack closure, and leads to a simple but effective modification of the NASGRO equation for fatigue crack growth. The approach is validated experimentally, and its application to the fitness-for-purpose assessment of surface-treated components is discussed.

Introduction

A very common approach to describe the crack growth behavior of long cracks is the NASGRO equation, which is based on the crack growth equation according to Forman and Mettu [2] considering plasticity-induced crack closure using the crack opening function f introduced by Newman [3]. The NASGRO equation is a powerful tool for estimating the growth rate of cracks which have already built up crack closure completely; however, it is not able to describe the behavior of short cracks [4]. Section 2 summarizes briefly how the build-up of crack closure can be modeled and implemented into the NASGRO equation so that the crack growth rate of short and long cracks can be estimated equally well. To investigate the crack arrest and crack growth behavior in the presence of residual stresses, experiments were performed on rolled flat bars. Section 3 describes how a residual stress field was introduced in the flat bars, how the corresponding crack growth threshold was determined, and gives a simple estimate for the threshold of a crack in the presence of residual stresses along with its experimental validation. Finally, section 4 shows how to compute the propagation of cracks of arbitrary length in arbitrary residual stress fields.

Nomenclature

Δa	crack extension
a_0	notch depth
a	total crack length
C	crack growth constant
$\mathrm{d}a/\mathrm{d}N$	fatigue crack growth rate
f	crack opening function
F	crack velocity factor
ΔK	stress intensity factor range
ΔK_0	stress intensity factor range for long crack growth at $R = 0$
ΔK_{th}	threshold of stress intensity factor range for crack propagation
$\Delta K_{\mathrm{th,eff}}$	intrinsic (effective) threshold stress intensity factor range
$\Delta K_{\mathrm{th,lc}}$	long crack growth threshold stress intensity factor range
K_{C}	fracture toughness
K_{max}	maximum stress intensity factor
l_i	fictitious length scales
m	Paris exponent
p, q	empirical constants describing the curvatures that occur near the threshold and near the instability region of the crack growth curve, respectively
R	load ratio
σ_{max}, σ_{min}	maximum, minimum stress
σ_{a}, σ_{r}	applied stress, residual stress (σ_{r} is equal to the mean stress for a load ratio of $R = -1$)

Modified NASGRO equation

Short cracks are able to grow below the threshold for long cracks, and they grow faster than long cracks at the same stress intensity factor range. The common NASGRO equation

$$\frac{\mathrm{d}a}{\mathrm{d}N} = C \cdot F \cdot \Delta K^m \cdot \frac{\left(1 - \frac{\Delta K_{\mathrm{th}}}{\Delta K}\right)^p}{\left(1 - \frac{K_{\mathrm{max}}}{K_{\mathrm{C}}}\right)^q} \tag{1a}$$

and its simplified form with $p = m$, $q = 1$ and $K_{\mathrm{max}} = \Delta K / (1 - R)$

$$\frac{\mathrm{d}a}{\mathrm{d}N} = C \cdot F \cdot \frac{(\Delta K - \Delta K_{\mathrm{th}})^m}{1 - \frac{1}{1-R}\frac{\Delta K}{K_{\mathrm{C}}}} \tag{1b}$$

are able to describe the three branches of the crack growth curve (see Fig. C.1b) in dependence of the load ratio $R = \sigma_{\min} / \sigma_{\max}$. To consider the behavior of short cracks, the crack velocity factor F (for short crack behavior in branch II, i.e., the Paris region) and the threshold for crack propagation ΔK_{th} (for short crack behavior below the threshold for long crack growth $\Delta K_{\mathrm{th,lc}}$) have to be modified. Fig. C.1a shows a simple mechanical model on which the following considerations are based. The total crack length a consists of the notch depth a_0 and the crack extension Δa. To calculate the stress intensity factor range ΔK the total crack length $a = a_0 + \Delta a$ is used, whereas for the build-up of crack closure – and hence for modeling of the transition from short to long crack behavior – only the crack extension Δa is responsible. An illustration of the build-up of crack closure for different crack closure mechanisms with fictitious length scales l_i is shown in Fig. C.1c.

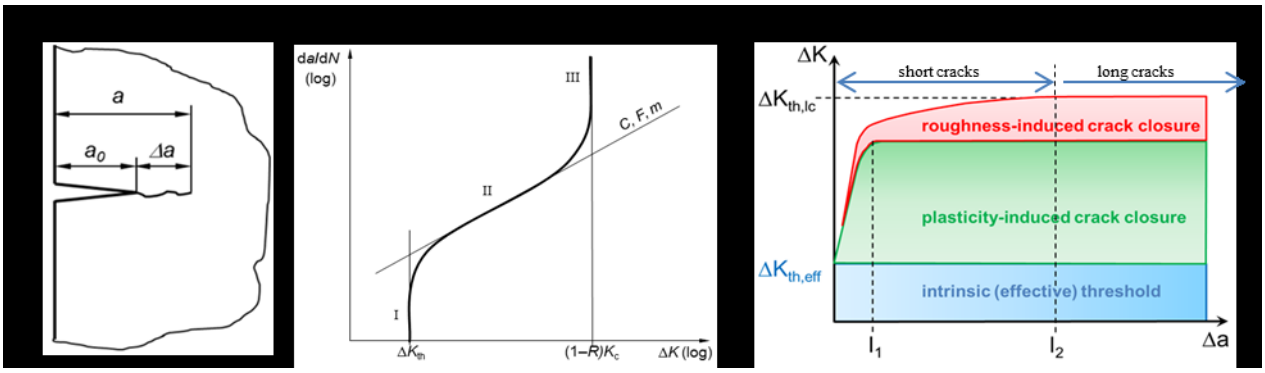

Fig. C.1: (a) illustration of mechanical model; (b) typical fatigue crack growth curve; (c) illustration of the build-up of crack closure.

To consider now the build-up of crack closure in the modified model, the material specific length scales l_i have to be determined. To this purpose, fatigue experiments to determine the crack resistance curve (R-curve, where ΔK_{th} is plotted against Δa) following the approach of Tabernig et al. [5], were performed. The length scales l_i were then fitted using the experimentally determined data. For the description of the build-up of crack resistance starting from $\Delta K_{\mathrm{th,eff}}$ at a crack extension of $\Delta a = 0$ to the long crack threshold $\Delta K_{\mathrm{th,lc}}$ at large Δa ($\Delta a >> \max(l_i)$), the empirical approaches

$$\Delta K_{\mathrm{th}} = \Delta K_{\mathrm{th,eff}} + \left(\Delta K_{\mathrm{th,lc}} - \Delta K_{\mathrm{th,eff}}\right) \cdot \left[1 - \sum_{i=1}^{n} v_i \cdot \exp\left(-\frac{\Delta a}{l_i}\right)\right] \tag{2}$$

for short crack behavior below the threshold for long crack growth and

$$F = 1 - \left(1 - \left(\frac{1-f}{1-R}\right)^{m}\right) \cdot \left[1 - \sum_{i=1}^{n} v_i \cdot \exp\left(-\frac{\Delta a}{l_i}\right)\right] \text{ with the constraint } \sum_{i=1}^{n} v_i = 1 \tag{3}$$

for short crack behavior in the Paris and near-threshold regime are proposed. More detailed information about the modified NASGRO equation for short cracks can be found in [4].

Influence of residual stresses

To investigate the crack growth in the presence of residual stresses, a specimen with a special geometry was developed (see Fig. C.2b). Extended areas of tensile as well as of compressive residual stresses were introduced by means of rolling (see Fig. C.2a). The rolling process deforms the specimen plastically below the areas of contact, in that case near the edges of the specimen. In that way, a residual stress field is generated that varies from high compressive residual stresses at the edges to lower tensile residual stresses in the middle of the specimen (see Fig. C.3). Subsequently, the specimen was tested under stepwise increasing constant load [5]. The crack growth rate was monitored and compared to the crack growth rate of a residual stress free specimen (both with an initial notch depth of 2 mm). As expected, the threshold for long crack growth of the specimen with residual stresses was several times higher than that of the residual stress free specimen (compare Fig. C.4, curves 1 and 5). This happens due to the high compressive residual stresses near the edges of the specimen. These compressive stresses cause the crack to be closed for a much higher portion of a load cycle compared to a residual stress free specimen at the same load ratio R. In Fig. C.4 the crack growth rates for a residual stress free specimen (curve 1) and for a specimen with residual stresses are plotted (curves 2-5). For the curves 2, 3 and 4, the crack initially grows slightly, but after a certain crack extension crack arrest occurs due to the combined influence of compressive residual stresses and build-up of crack closure. Finally, the applied load is high enough to overcome the threshold so that the crack grows continuously, i.e., the threshold for long crack growth is reached (curve 5).

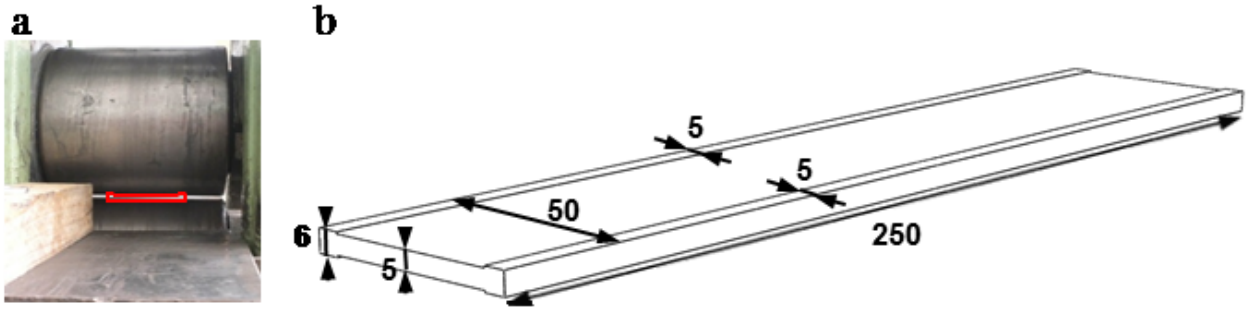

Fig. C.2: (a) rolling mill; (b) specimen geometry for fatigue crack growth experiments with residual stress zones (dimensions in mm).

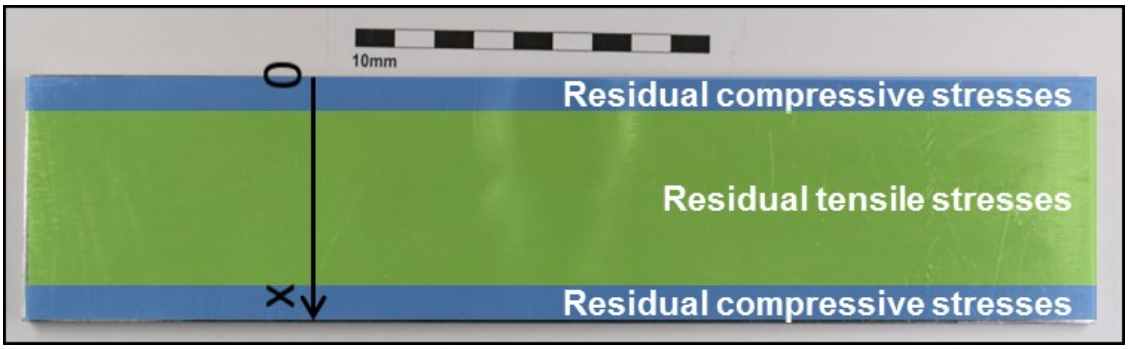

Fig. C.3: Illustration of the residual stress areas across the specimen width.

To estimate the long crack threshold of the specimen with residual stresses, the combined influence of applied stress amplitude σ_a and residual stress σ_r has to be considered. A simple approximation for the dependence of the long crack threshold on the load ratio R was given by Gänser et al. [6] as

$$\Delta K_{\mathrm{th,lc}} = \Delta K_0 \cdot (1 - R), \quad R = \frac{\sigma_{\min}}{\sigma_{\max}} = \frac{\sigma_r - \sigma_a}{\sigma_r + \sigma_a}, \tag{4}$$

see Fig. C.5b. The residual stress $\sigma_r(x)$ was determined experimentally using the cut-compliance method [1]. A comparison of the measured residual stress field with the results from a simplified finite-element simulation of the rolling process is shown in Fig. C.5a.

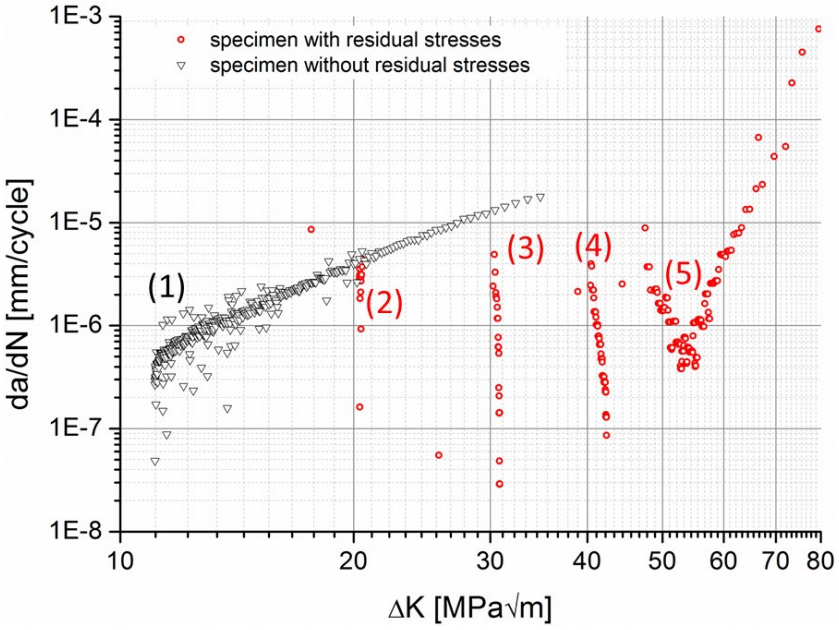

Fig. C.4: Comparison between the crack growth rate in a residual stress free specimen and in a specimen with residual stresses, both with an notch depth of 2 mm, tested at a load ratio R = -1; start parameters of the curves: curve (1): ΔK = 11 MPa m$^{0.5}$, a = 3.50 mm; curve (2): ΔK = 20 MPa m$^{0.5}$, a = 2.19 mm; curve (3): ΔK = 30 MPa m$^{0.5}$, a = 2.28 mm; curve (4): ΔK = 40 MPa m$^{0.5}$, a = 2.39 mm; curve (5): ΔK = 50 MPa m$^{0.5}$, a = 2.65 mm.

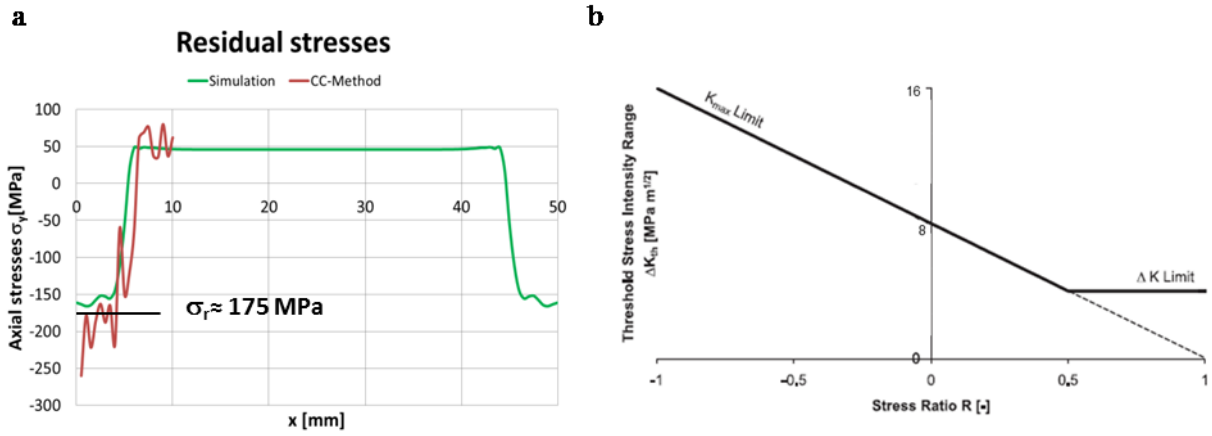

Fig. C.5: (a) due to rolling introduced residual stresses in axial direction; (b) dependence of crack growth threshold on the stress ratio.

For the approximation of the long crack threshold the area of interest is in a depth of x = 2 mm depth (notch depth). Here the measured compressive residual stresses are about 175 MPa. The applied load σ_a after the final load increase is also known with 257 MPa. Inserting these

data into Eq. (4) leads to a threshold of 50.2 MPa√m, which is in good agreement with the experiment (curve 5 in Fig. C.4).

Extension to general residual stress field

After having computed the influence of residual stresses on the crack arrest behavior under a constant residual stress which is equivalent to a mean stress (section 4, Eq. (4)), we seek now to extend our reasoning to the arrest and growth behavior of cracks of arbitrary length in arbitrary stress fields. To this purpose, we refer again to the influence of the residual stresses σ_r on the load ratio R as in the previous section; however, in the general case the local variation of σ_r has to be taken into account. The minimum and maximum local stresses during one load cycle are calculated at each position x by superposition of cyclic load stresses and residual stresses,

$$\sigma_{\min}(x) = \sigma_{\min,a}(x) + \sigma_r(x), \quad \sigma_{\max}(x) = \sigma_{\max,a}(x) + \sigma_r(x) \ . \tag{5}$$

Knowing the minimum and maximum local stresses, the minimum and maximum crack tip loading during one load cycle can be estimated using an influence function according to Tada [7]:

$$K_{\min}(a) = \frac{2 \cdot Y}{\sqrt{\pi \cdot a}} \int_0^a \frac{\sigma_{\min}(x)}{\sqrt{1 - \left(\frac{x}{a}\right)^2}} \mathrm{d}x, \quad K_{\max}(a) = \frac{2 \cdot Y}{\sqrt{\pi \cdot a}} \int_0^a \frac{\sigma_{\max}(x)}{\sqrt{1 - \left(\frac{x}{a}\right)^2}} \mathrm{d}x \ . \tag{6}$$

Finally, the stress intensity factor range and the load ratio at the crack tip for a crack of length a are obtained as $\Delta K(a) = K_{\max}(a) - K_{\min}(a)$ and $R(a) = K_{\min}(a) / K_{\max}(a)$, respectively are obtained. If $\Delta K(a)$ is below the threshold ΔK_{th} for the given crack length a and load ratio $R(a)$, crack arrest occurs. If the threshold is exceeded, the crack growth rate for any given crack length a in any given residual stress field $\sigma_r(a)$ can be calculated via Eqns (1) – (3).

Acknowledgements

Financial support by the Austrian Federal Government (in particular from Bundesministerium für Verkehr, Innovation und Technologie and Bundesministerium für Wirtschaft, Familie und Jugend) represented by Österreichische Forschungsförderungsgesellschaft mbH and the Styrian and the Tyrolean Provincial Government, represented by Steirische Wirtschaftsförderungsgesellschaft mbH and Standortagentur Tirol, within the framework of the COMET Funding Programme is gratefully acknowledged.

References for Publication C

[1] Cheng, W., Finnie, I., 1994. An overview of the crack compliance method for residual stress measurement, 4th Int Conf. On Residual Stress, Baltimore, p. 449-458.

[2] Forman, R.G., Mettu, S.R., 1992. Behavior of surface and corner cracks subjected to tensile and bending loads in Ti-6Al-4V alloy. In: Fracture Mechanics: 22nd Symposium, Vol. 1 (Eds H.A. Ernst, A. Saxena, D.L. McDowell), ASTM STP 1131, American Society for Testing and Materials, Philadelphia, p. 519-546.

[3] Newman, J.C., 1984. A crack opening stress equation for fatigue crack growth, Int J Fract, 24:R131-5.

[4] Maierhofer, J., Pippan, R., Gänser, H.-P., 2014. Modified NASGRO equation for physically short cracks, Int J Fatigue, Vol. 59, p. 200-207.

[5] Tabernig, B., Powell, P., Pippan, R., 2000. Resistance curves for the threshold of fatigue crack propagation in particle reinforced aluminium alloys, Fatigue crack growth thresholds, endurance limits, and designs, ASTM STP 1372, J.C. Newman, Jr. and R.S. Piascik, Eds., American Society for Testing and Materials, West Conshohocken, PA.

[6] Gänser, H.-P., Leitgeb, A., Glinsner, K., Eichlseder, W., 2007. Computation of a modified Haigh-Goodman diagram for damage tolerant design for infinite fatigue life, Proc. IMechE Vol 221 Part C: J. Mechanical Engineering Science, p. 619-623.

[7] Tada, H., Paris, P.C., Irwin, G.R., 2000. The stress analysis of cracks handbook, third edition, American Society of Mechanical Engineers, New York.

Publication D: Modified Kitagawa-Takahashi diagram – a practical modelling approach

Modified Kitagawa-Takahashi diagram – a practical modelling approach

J. Maierhofer[1,2], H.-P. Gänser[1], R. Pippan[2]

[1]Materials Center Leoben Forschung GmbH, Roseggerstraße 12, A-8700 Leoben;
juergen.maierhofer@mcl.at; hans-peter.gaenser@mcl.at
[2]Erich Schmid Institute of Materials Science, Jahnstraße 12,A-8700 Leoben;
reinhard.pippan@oeaw.ac.at

Abstract

The Kitagawa-Takahashi diagram in its commonly used form allows to predict, for cracks of given length and stress range, the allowable stress range for infinite life. However, caution is advised if a crack emanates not directly from the plane surface but from a sharp, crack-like notch instead. In this contribution, it is shown that taking the crack length equal to the total flaw depth (sum of notch depth and crack length) gives non-conservative results. Based on a simple mechanical model, a 3-dimensional Kitagawa-Takahashi diagram considering the build-up of crack growth resistance as well as the influence of the notch depth is developed. Comparison of model predictions and experimental results shows good agreement.

Introduction

The Kitagawa-Takahashi (KT) diagram [1] is a widespread tool for fracture mechanics based design of components and fracture control concepts such as the safe-life or fail-safe concepts. It combines the fatigue crack growth threshold and the fatigue endurance limit into a single plot, thereby defining the area of non-propagating cracks (leading to infinite fatigue life). Using the fictitious intrinsic crack length $a_{0,\mathrm{H}}$ introduced by El Haddad [2], a smooth transition from the threshold of long cracks to the endurance limit is given (Fig. D.1). This intrinsic length is computed as

$$a_{0,\mathrm{H}} = \frac{1}{\pi}\left(\frac{\Delta K_{\mathrm{th,lc}}}{Y \cdot \Delta\sigma_{\mathrm{e}}}\right)^2 \tag{1}$$

and the endurance limit stress range dependent on the crack size a – i.e., the threshold stress range for crack propagation – is calculated by

$$\Delta\sigma_{\mathrm{th}}(a_{0,\mathrm{H}}) = \frac{\Delta K_{\mathrm{th,lc}}}{Y \cdot \sqrt{\pi \cdot \left(a + a_{0,H}\right)}}\,, \tag{2}$$

where $\Delta K_{\mathrm{th,lc}}$ denotes the fatigue crack growth threshold for long cracks, $\Delta\sigma_{\mathrm{e}}$ the endurance limit stress range of polished specimens without flaws, and Y is the geometry factor of the crack.

However, for cracks which have not built up crack closure completely (short cracks) the threshold of stress intensity range can be significantly smaller [3-7] and as a consequence the approximation according to El Haddad is non-conservative. So the build-up of crack closure has to be considered in the KT diagram. One method to describe the build-up of crack closure was proposed by McEvily [8], using an exponential function. Chapetti [9] used this exponential function to calculate the threshold stress for physically short cracks and showed that the threshold stress prediction obtained using the El Haddad correction is partially significantly higher, and therefore non-conservative. Similar behaviour has been shown by Tabernig [10]. In other words, the endurance limit stress for physically short cracks is smaller than that one predicted using the intrinsic length scale $a_{0,\mathrm{H}}$ according to El Haddad (see Fig. D.1).

Nomenclature

Δa	crack extension length	l_i	fictitious length scales
a_0	notch depth	R	load ratio
$a_{0,H}$	fictitious intrinsic length scale following El Haddad	$\Delta\sigma$	stress range
a	total crack length	$\Delta\sigma_e$	endurance limit stress range of polished specimens without flaws
ΔK	stress intensity factor range	$\Delta\sigma_{th}$	threshold stress range for crack propagation
ΔK_{th}	threshold of intensity factor range for crack propagation	$\Delta\sigma_{th,lc}$	threshold stress range for crack propagation calculated using $\Delta K_{th,lc}$
$\Delta K_{th,eff}$	intrinsic (effective) threshold stress intensity factor range	v_i	weighting factors
$\Delta K_{th,lc}$	long crack growth threshold stress intensity factor range		

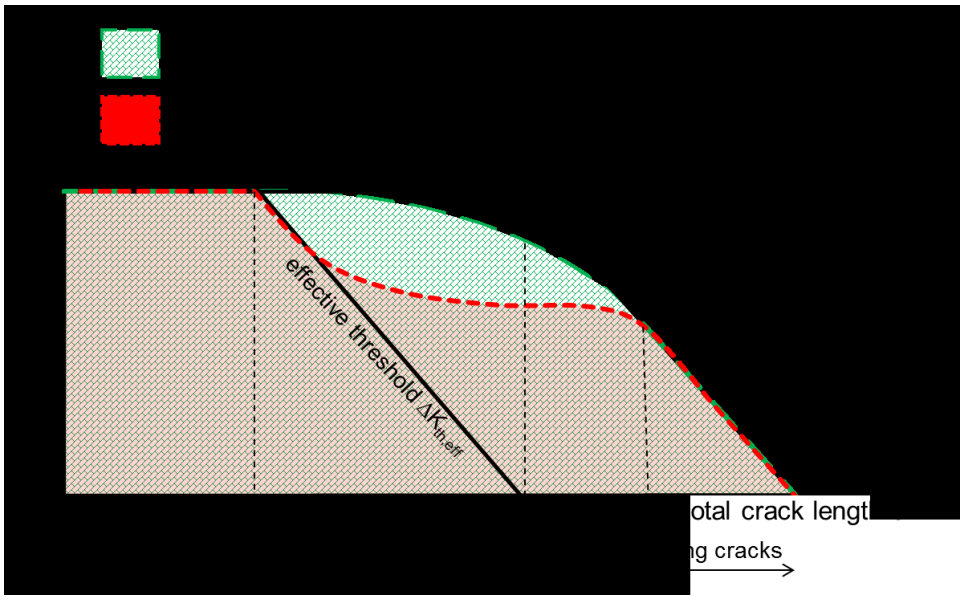

Fig. D.1: Kitagawa-Takahashi diagram, showing the areas of non-propagating cracks according to El Haddad and Chapetti, respectively.

However, whereas Chapetti's approach to the KT diagram accounts for short crack effects, it still neglects the influence of the depth of a pre-existing flaw (which may be conveniently

regarded as a sharp notch). In order to avoid non-conservative predictions, especially in the context of fracture control concepts, it is indispensable to account for effects due to the initial flaw. Tanaka and Akiniwa [7] investigated experimentally the influence of notch depth on the KT diagram and showed that the region of non-propagating cracks becomes smaller with increasing initial notch depth. In this paper, a modified KT diagram is developed that accounts for all of the aforementioned effects and is therefore readily applicable in the context of fracture control concepts in mechanical design.

Build-up of crack closure

The model for the build-up of crack closure at the threshold as proposed by the authors in [11] is based on a simple mechanical model as shown in Fig. D.2.

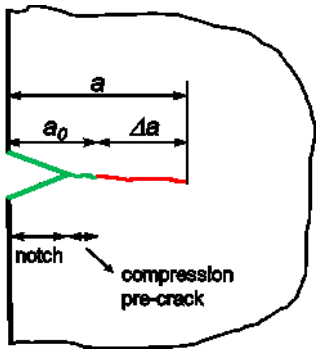

Fig. D.2: Schematic illustration of the proposed mechanical model: emanating from a deep sharp notch a_0, a crack of extension Δa grows. Only on this crack extension Δa the build-up of crack closure is possible.

To calculate the stress intensity factor

$$\Delta K = Y \cdot \Delta\sigma \cdot \sqrt{\pi \cdot a} \tag{3}$$

the total crack length

$$a = a_0 + \Delta a \tag{4}$$

is used, which is a combination of notch depth a_0 and crack extension Δa.

In contrast, for the build-up of crack closure not the total crack length a should be used, except the crack starts immediately at the surface of a component ($a_0 = 0$). If a crack starts

from a notch (e.g., real design notches, casting defects or notches caused due to a forging lap, inappropriate handling, foreign object damage, et cetera) Δa must be used, because the crack flanks can be in contact only over this length. In other words, the notch depth a_0 is not subject to any crack closure even under compression loading; only by the crack extension Δa the build-up of crack closure is possible.

For the description of the threshold build-up starting from the intrinsic value of $\Delta K_{\mathrm{th,eff}}$ at a crack extension of $\Delta a = 0$ to the long crack growth threshold $\Delta K_{\mathrm{th,lc}}$ at large Δa, the empirical approach

$$\Delta K_{\mathrm{th}} = \Delta K_{\mathrm{th,eff}} + (\Delta K_{\mathrm{th,lc}} - \Delta K_{\mathrm{th,eff}}) \cdot \left[1 - \sum_{i=1}^{n} v_i \cdot \exp\left(- \frac{\Delta a}{l_i} \right) \right] \tag{5}$$

with the constraint

$$\sum_{i=1}^{n} v_i = 1 \tag{6}$$

is used [11]. The l_i can be interpreted as fictitious length scales for the formation of crack closure effects (see Fig. D.3), similar to El Haddad's $a_{0,\mathrm{H}}$, and determined in conjunction with the v_i by fitting experimentally determined crack resistance curves (where ΔK_{th} is plotted against Δa). Such crack resistance curves may be obtained, e.g., from SENB specimens with different notch depth, using the constant load increasing technique following the approach of Tabernig et al. [10]. The description of the increase of ΔK_{th} with crack length is in principle similar to the idea of McEvily [8]. However, the different l_i in this approach take into account that different crack closure mechanisms need different lengths to build up completely.

Considered example material

As material for the experimental investigations, the QT steel 25CrMo4 was chosen. The material has a bainitic microstructure and a hardness of ~245 HV10. In the tensile test, a 0.2% offset yield stress of 512 MPa, a tensile strength of 674 MPa, and an elongation at fracture of 18.9% are obtained. In Fig. D.4 the crack resistance curve of the material is shown.

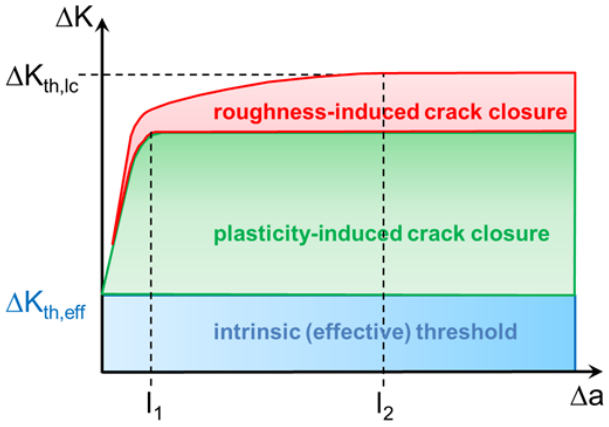

Fig. D.3: Illustration of the crack resistance curve caused by two different closure mechanisms; each closure mechanism is built up completely over a specific crack extension (described by the fictitious length scales l_i).

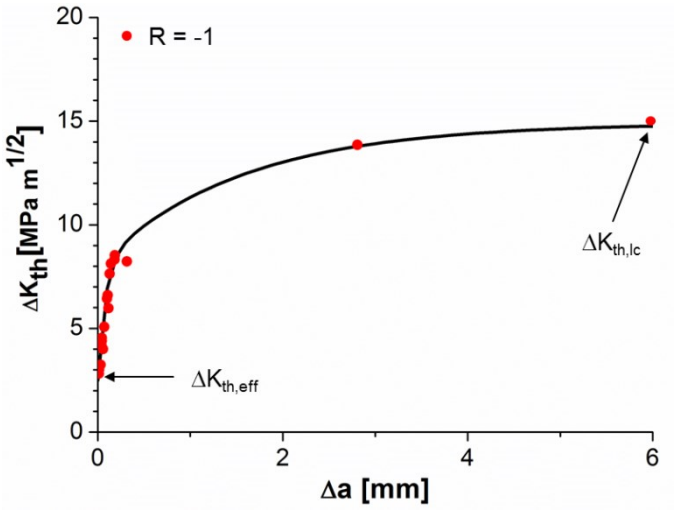

Fig. D.4: Crack resistance curve: experimental data points and analytically estimation curve from Eq. (5).

Considering various notch depths in the KT diagram

The threshold stress range for crack propagation considering the model for build-up of crack closure introduced in Section 2 can now be calculated using Eqns (3-5):

$$\Delta\sigma_{\mathrm{th}} = \min\left(\frac{\Delta K_{\mathrm{th,eff}} + (\Delta K_{\mathrm{th,lc}} - \Delta K_{\mathrm{th,eff}}) \cdot \left[1 - \sum_{i=1}^{n} v_i \cdot \exp\left(-\frac{\Delta a}{l_i} \right) \right]}{Y \cdot \sqrt{\pi \cdot (a_0 + \Delta a)}}, \Delta\sigma_{\mathrm{e}} \right), \tag{7}$$

where for very small total crack lengths the threshold stress range is limited by the fatigue endurance limit of polished specimens without flaws $\Delta\sigma_{\mathrm{e}}$.

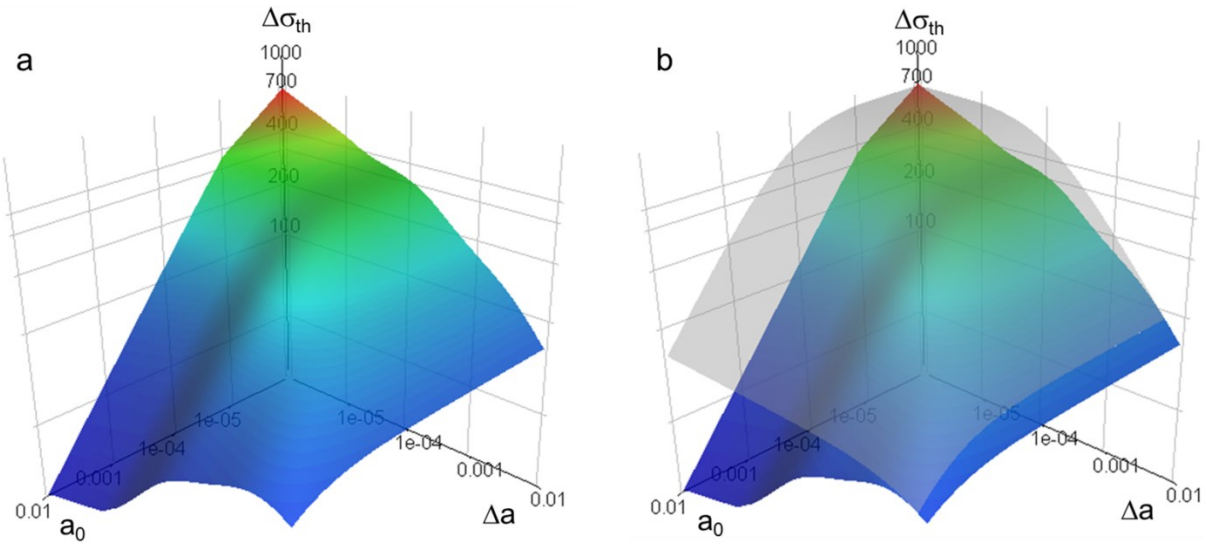

Fig. D.5: Threshold stress range $\Delta\sigma_{\mathrm{th}}$ plotted over crack extension Δa and notch depth a_0 (three-dimensional Kitagawa-Takahashi diagram).

Using Eq. (7), the threshold stress range for any notch depth a_0 and crack extension Δa can now be determined. In Fig. D.5a, a three-dimensional extension of the KT diagram is shown, varying both the notch depth a_0 and the crack extension Δa. In Fig. D.5b, in addition the conventional threshold stress range

$$\Delta\sigma_{\mathrm{th,lc}} = \frac{\Delta K_{\mathrm{th,lc}}}{Y \cdot \sqrt{\pi \cdot (a_0 + \Delta a + a_{0,\mathrm{H}})}} \tag{8}$$

calculated using El Haddad's approach, Eq. (2), is plotted (grey surface). It is assumed that a_0 and Δa are small compared to the component size, and that the stress gradients are small. A comparison between these surfaces shows that they are congruent for long crack extensions Δa (i.e. for cracks which have built up their crack closure completely). However, for short crack extensions a lifetime estimation based on El Haddad's approach can lead to non-conservative results, because crack propagation is possible also at stress ranges far below the

limit given by Eq. (8) (and actually most likely, as Fig. D.5b implies). To emphasize the difference between the conventional KT diagram and the new approach, cuts have been made through this 3-dimensional illustration of the KT-diagram along the a_0 and Δa directions. Fig. D.6 shows one at a constant notch depth (a_0 = 1 mm, green curve) and another at a constant crack extension (Δa = 1 mm, red curve). The black lines represent the respective intersections with the non-conservative threshold stress range according to Eq. (8). Here, the cuts were also done at constant notch depth or constant crack extension, respectively, of 1 mm.

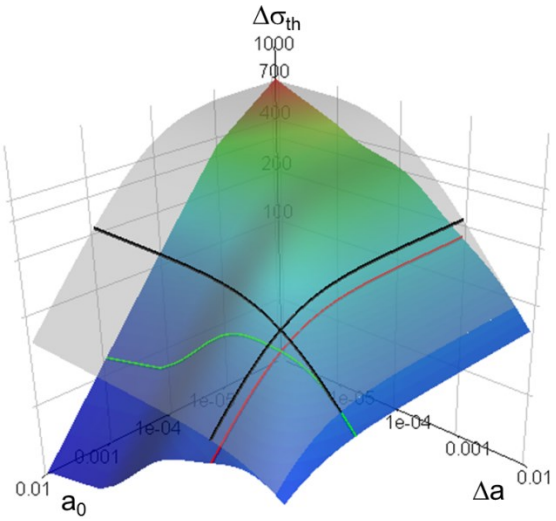

Fig. D.6: Cuts in the 3-dimensional KT diagram at constant notch depth a_0 = 1 mm and at constant crack extension Δa = 1 mm, respectively

A comparison of these curves shows clearly why it is useful to account separately for notch depth a_0 and crack extension Δa, and therefore to introduce an additional axis in the KT diagram. In Fig. D.7a the cuts from Fig. D.6 are compared. The total crack length $a = a_0 + \Delta a$ of all curves is identical for each point on their respective abscissae. However, the green curve deals with a constant notch depth a_0 and increasing crack extension Δa, whereas the red curve deals with constant crack extension and increasing notch depth. The black curve is, due to the symmetry of Eq. (8), identical for increasing a_0 and increasing Δa.

The region of non-propagating cracks predicted from Eq. (7) for a constant notch depth (under the green curve) is now completely different to the region predicted from a constant crack extension (under the red curve), although the total crack length a is the same for each point of the abscissa. As the fatigue crack builds up crack closure only with increasing crack extension Δa, the green curve starts at a low limit of stress ranges where no crack propagation occurs

corresponding to the intrinsic crack growth threshold and increases gradually due to the build-up of closure until it reaches the long crack prediction given by the inclined branch of the black curve. The red curve for constant crack extension Δa = 1 mm lies somewhat below the conventional El Haddad prediction (Eq. (8), black curve) as crack closure is not yet fully developed at Δa = 1 mm. In contrast, Fig. D.7b shows the analogous curves for a_0 = 5 mm and Δa = 5 mm. Here, crack closure is fully developed for the red curve, and so this curve is identical to the conventional El Haddad prediction. The green curve shows again the gradual build-up of crack closure until it approaches the long crack prediction.

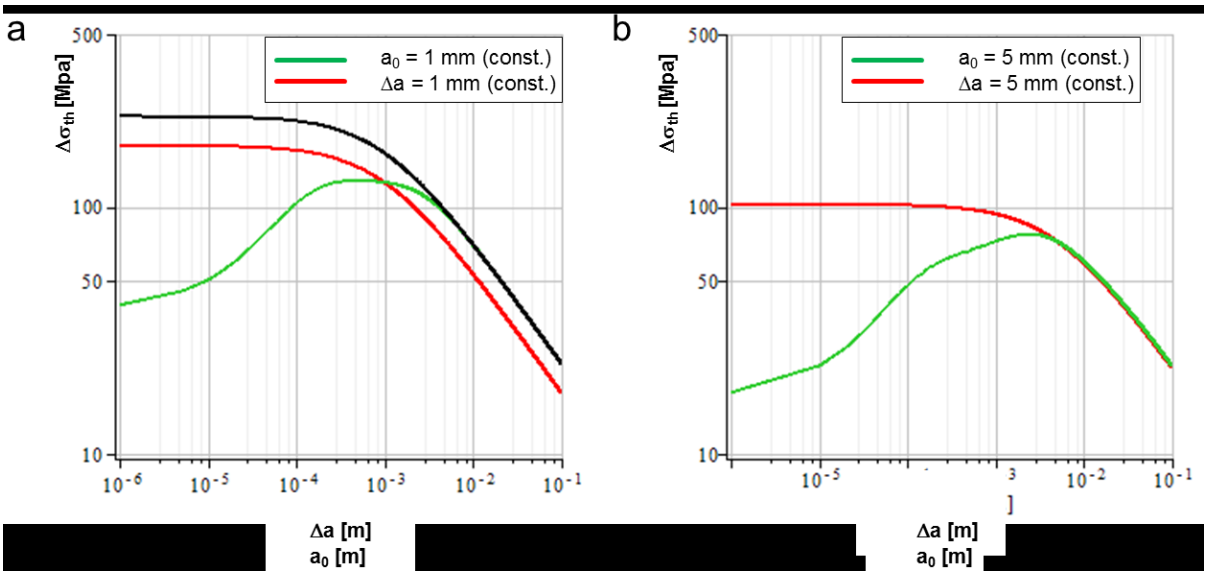

Fig. D.7: Comparison of two cracks with the same total crack length a - the green line for a constant notch depth varying the crack extension and the red line with a constant crack extension varying the notch depth. The conventional prediction following El Haddad, Eq. (8), is shown in black.

If one plots the intrinsic threshold for crack propagation $\Delta K_{th,eff}$ and the long crack threshold for crack propagation $\Delta K_{th,lc}$ in a double logarithmic diagram against the total crack length $a = a_0 + \Delta a$, it is rather easy to estimate the limiting curves for non-propagating cracks. The threshold stress range $\Delta\sigma_{th}$ of non-propagating cracks of total length $a = a_0$, extension $\Delta a = 0$, and therefore non-existent closure, is given by:

$$\Delta\sigma_{th}(a = a_0) = \frac{\Delta K_{th,eff}}{Y \cdot \sqrt{\pi\, a_0}} \qquad (9)$$

Now it depends on the length of the notch how steep the limiting curve is in the beginning. The deeper a notch, the steeper is the initial increase of the limiting curve. After a certain increase the limiting curve becomes shallower and finally approaches the asymptotic line given by the long crack threshold $\Delta K_{th,lc}$, see also Fig. D.8. Here for different notch depths the associated limiting curve for non-propagating cracks are plotted over the total crack length a. The curves are limited by an upper bound due to the endurance limit.

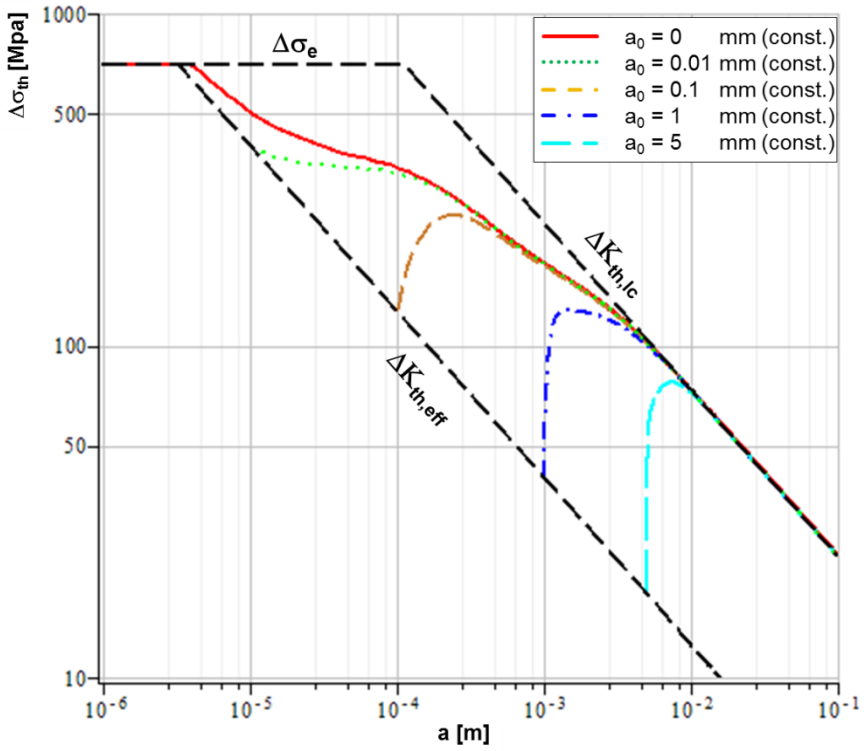

Fig. D.8: Limiting curves for non-propagating cracks in dependence of notch depth a_0 and total crack length $a = a_0 + \Delta a$.

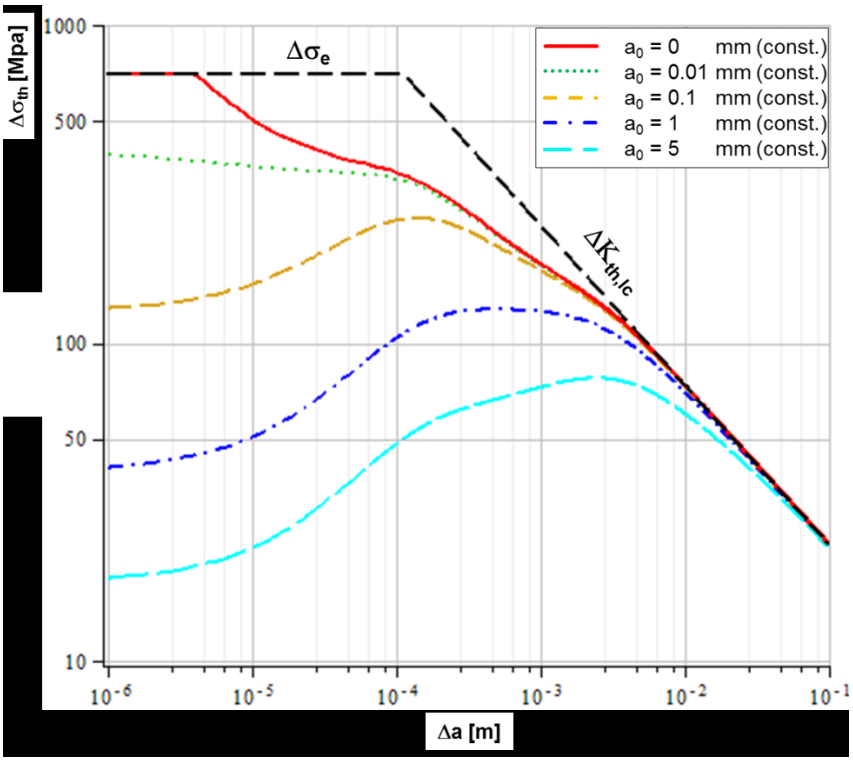

Fig. D.9: Threshold stress range against crack extension emanating from different notch depths.

In Fig. D.9, the threshold stress range for various notch depths a_0 is plotted against the crack extension Δa only. One can see that, for shallow notches, crack closure is not built up sufficiently fast to generate cracks which stop after a certain crack extension. That means that the region of non-propagating cracks (the area below the threshold stress range) is much larger for cracks emanating from a shallow notch or from a smooth surface than for cracks emanating from deep notches.

Moreover, from this figure one can easily extract the allowable crack extension for a given applied stress range. Supposed we have an applied stress range of 100 MPa and a notch of 1 mm depth. For these conditions the crack is able to grow until a crack extension of approximately 0.1 mm is reached. Then the crack will arrest, whereas for a notch of 5 mm depth an applied stress range of 100 MPa would lead to finite life (the corresponding curve for non-propagating cracks does not reach the value of 100 MPa).

To verify the model predictions, experiments with three different notch depths (0.813 mm, 2.19 mm and 5.39 mm) were performed. In Fig. D.10 the theoretically possible crack

extensions due to the predicted threshold stress curves are drawn as red dashed lines. The crack can grow until the crack extension Δa intersects the predicted threshold curve, where crack arrest occurs. Subsequently, the load may be increased until either crack arrest occurs again or the crack propagates to finite life. The experimentally determined crack extensions until crack arrest occurs are drawn as green points in the diagrams. As can be seen from Fig. D.10, good agreement between model predictions and experiment is observed.

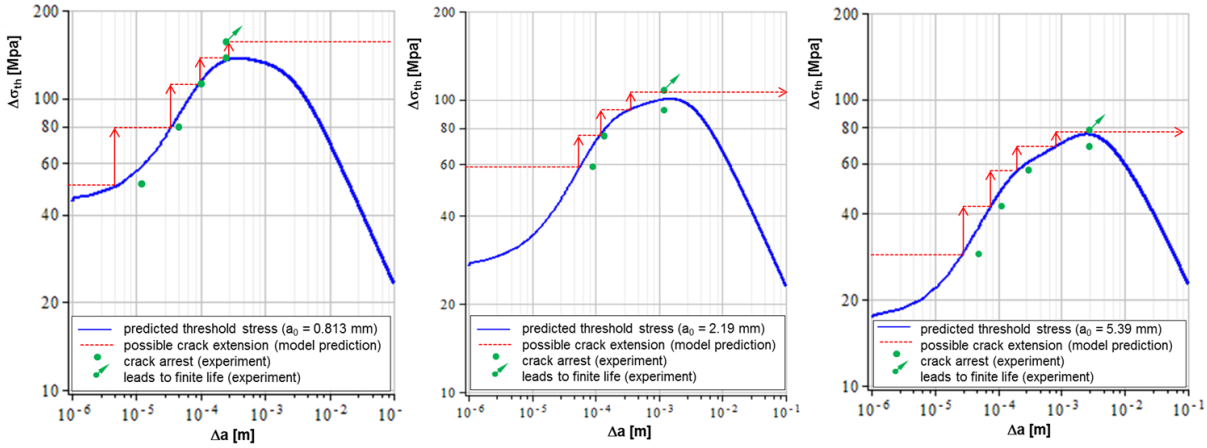

Fig. D.10: Comparison of the crack extension predicted from the threshold stress range with experimental results for samples with different notch depths a_0 = 0.81, 2.19, 5.39.

Conclusions

Based on a simple mechanical model, a 3-dimensional KT diagram was proposed considering the fact that a crack consists of two different contributions, namely the notch depth where fracture surface contact does not take place and a real crack extension. It was shown that it depends on both contributions – rather than only on their sum – whether a crack is in the area of non-propagating cracks or in the finite life area. Finally, the modified KT diagram was verified using experimental data. Special attention has to be paid to the fact that the deeper the initial notch is compared to the total crack length, the lower is the resistance against crack propagation. If one does not consider this marked influence of the initial notch depth, the endurance limit of a component may be severely over-estimated. In this respect, the modified KT diagram is expected to become a useful tool for the damage tolerance assessment of notched components.

Acknowledgements

Financial support by the Austrian Federal Government (in particular from Bundesministerium für Verkehr, Innovation und Technologie and Bundesministerium für Wirtschaft, Familie und Jugend) represented by Österreichische Forschungsförderungsgesellschaft mbH and the Styrian and the Tyrolean Provincial Government, represented by Steirische Wirtschaftsförderungsgesellschaft mbH and Standortagentur Tirol, within the framework of the COMET Funding Programme is gratefully acknowledged.

References for Publication D

[1] Kitagawa H, Takahashi S. Applicability of fracture mechanics to very small cracks or cracks in the early stage. In: Proceeding of the second international conference on mechanical behavior of materials, ASM; 1976. p. 627-31.

[2] El Haddad MH, Topper TH, Smith KN. Prediction of non-propagating cracks. Eng Fract Mech 1979;11: p. 573-84.

[3] S. Suresh, R.O. Ritchie. Propagation of short fatigue cracks. Int Metals Reviews (1984), Vol 29 No 6.

[4] R. Pippan, M. Berger, H.P. Stüwe. The influence of crack length on fatigue crack growth in deep sharp notches. Metall Trans 18A (1987), 429-435.

[5] J.C. Newman, E.P. Phillips, M.H. Swain. Fatigue-life prediction methodology using small-crack theory. Int J Fatigue (1999), Vol 21, Issue 2, 109-119.

[6] Richtie RO. Mechanisms of fatigue crack propagation in metals, ceramics and composites: the role of crack tip shielding. Mater Sci Engng 1988;103:15-88.

[7] Tanaka K, Akiniwa Y. Resistance-curve method for predicting propagation threshold of short fatigue crack at notches. Eng Fract Mech 1988;30(6): p. 863-76.

[8] McEvily AJ, Minakawa K. On crack closure and the notch size effect in fatigue. Eng Fract Mech 1987;28: p. 519-27.

[9] Chapetti MD. Fatigue propagation of short cracks under constant amplitude loading. Int J Fat 2003;25(12): p. 1319-26.

[10] Tabernig B, Powell P, Pippan R. Resistance curves for the threshold of fatigue crack propagation in particle reinforced aluminium alloys. Fatigue crack growth thresholds, endurance limits, and designs, ASTM STP 1372, J.C. Newman, JR. and R.S. Piascik, Eds., American Society for Testing and Materials, West Conshohocken, PA.

[11] Maierhofer J, Pippan R, Gänser HP. Modified NASGRO equation for physically short cracks. Int J Fat 2014;59: p. 200-07.